Journal of Applied Fluid Mechanics, Vol. 17, No. 5, pp. 1052-1072, 2024.
Available online at www.jafmonline.net, ISSN 1735-3572, EISSN 1735-3645.
https://doi.org/10.47176/jafm.17.05.2231

Effect of Synthetic Jet on NACA0012 Airfoil Vortex Structure and Aerodynamic Characteristics

J. Wang[1], X. Shi[1], Q. Zhang[2,3] and J. Chang[2,3†]

[1] *School of Environment and Safety Engineering, North University of China, Taiyuan, Shanxi, 030051 China*
[2] *College of Mechatronic Engineering, North University of China, Taiyuan, Shanxi, 030051, China*
[3] *Institute of Intelligent Weapons, North University of China, Taiyuan, Shanxi, 030051, China*

†Corresponding Author Email: changjl@nuc.edu.cn

ABSTRACT

In this manuscript, the vortex generated by the main frequency excitation of the shedding vortex at various attack angles is investigated by employing the synthetic jet control technique. We also analyzed the impact of the vortex structure on the fled flow around the wing and the spectral characteristics corresponding to the vortex. The dominant frequency and harmonic frequency corresponding to the wave rule of the shedding vortex at various attack angles without the absence of a synthetic jet are selected as the synthetic jet excitation frequency. The results indicate that under the excitation of fixed frequency synthetic jet, the shape of the shedding vortex in the flow field turns correspondingly. Compared with the flow field without jet excitation, it is found that the field with the jet at most attack angles is stable in 2S (Single) mode, and the flow field at a small attack angle is stable in a chaotic state. The angle of attack with a chaotic state is delayed by adding a jet, which makes the curves and corresponding spectral characteristics more orderly. At a defined attack angle, the combined frequency synthetic jet will cause the lift coefficient to fluctuate regularly. At this time, the multiple small-scale vortex structures lead to lift reduction.

Article History

Received August 16, 2023
Revised November 20, 2023
Accepted December 7, 2023
Available online February 24, 2024

Keywords:

Shedding vortex frequency
Synthetic jet frequency
Unsteady flow
Wake shedding
Active flow control

INTRODUCTION

Aircraft is the best means of transportation for long-distance travel, which has changed human history and way of thinking. The technological progress of aircraft has driven the vigorous development of a number of high-tech industries (Klochkov & Kritskaya, 2017). The development of the world economy has freed itself from the constraints of distance. Flight safety is extremely important for aircraft, and few passengers can survive an air crash (Fala, 2022). The wings of aircraft are the main source of aircraft lift, and the aerodynamic performance of aircraft wings will be reduced due to the flow separation. Flow separation will threaten the stability and safety of aircraft flight (Nguyen et al., 2022). The effects of the average attack angle and pitch frequency on instantaneous forces and vortex structures were studied by Kurtulus (2019), and the results showed that the oscillation of the airfoil can change the amplitude of aerodynamic load oscillation.

There are many differences between low Reynolds number and typical Reynolds number (Re>10^6) in flow structure and characteristics of aircraft. According to Gupta et al. (2023) research, there are three modes of wake: continuous vortex sheet mode, alternating vortex shedding mode, and alternating vortex pair shedding mode. The reverse pressure gradient makes the air flow easy to separate from the wall, forming a laminar separation shear layer. As a result of the K-H instability, the laminar flow shear layer transits, generating a turbulent separated shear layer. The laminar separation bubble flow structure is generated by the separated airflow quickly returning to the wall and reattaching to the wall, taking the shape of a turbulent boundary layer, which can significantly decrease wing performance, lift loss, increase drag, wing shaking, and even stall.

Therefore, reducing the flow separation is one method to improve the aerodynamic characteristics of the airfoil. The position and extent of airflow separation would directly affect the performance of airfoils. Understanding the structure of airfoil flow vortices during flow separation is considered accelerating the progress of aircraft wings. The two ways to control flow separation are as follows: active control and passive control. Passive control reduces the degree of flow separation by changing the parameters of the wing. Active flow control is done by changing the flow environment. Synthetic jets can be summarized in active flow control technology. The advantage of synthetic jets to control flow separation is that the energy can be concentrated in a wide range for precise control, and better control of flow separation can be achieved with less energy.

NOMENCLATURE

α	angle of attack	∇p	pressure gradient
f	expression of excitation function of synthetic jet	G_b	generation of turbulent kinetic energy due to buoyancy
G_k	generation of turbulent kinetic energy due to the average velocity gradient	ω	dissipation rate
Re	Reynolds number	ρ	density
t	time	u	velocity flow field vector
u_t	turbulent viscosity coefficient	u_x	velocity vector of the flow field along the x-direction component of the global coordinate system
u_y	velocity vector of the flow field along the y-direction component of the global coordinate system	u_z	velocity vector of the flow field along the z-direction component of the global coordinate system
v	kinematic viscosity of the fluid, respectively	Y_M	influence of compressible turbulent pulsation expansion on the total dissipation rate
Y+	dimensionless wall distance		

The frequency characteristics of shedding vortices generated by airflow separation at Re=10000 were studied by Chang et al. (2022). This study found that with the attack angle increasing, the frequency of shedding vortices becomes more complex. The principle of flow separation and laminar to turbulent transition in the aerodynamic profile separation shear-layer was researched by Rodríguez et al. (2013). The impression of the lift and drag coefficient was studied through numerical simulation of active diaphragm control by Di et al. (2017). Arif & Hasan (2021) concluded the influence of warming on the average lift and drag coefficient at Re=100. The results showed that at low to medium values of Re, the initial laminar shear layer transited to turbulence, and the finally formed vortex shedding formed a vortex street similar to Von Karman vortices in the backwash. The flow mechanism and the causes of laminar separation vortices were deeply explored by AlMutairi et al. (2017). The flow oscillation was caused by the quasi-periodic burst and recombination of the shedding vortex. When the shedding vortex was attached to the wing, its turbulent kinetic energy was maximum, whereas the length of the shedding vortex was the shortest. According to Kurtulus (2015), the situation of the flow field and the vortices at Re=1000 of the NACA0012 were investigated. Pradhan et al. (2022) explored the influence of flow field size and length-width ratio on convection and aerodynamic characteristics. From the results, it is obvious that the lift coefficient is the highest at an attack angle of 8°. If the attack angle is more than 8°, the force acting on the wing will oscillate. The formation and shedding of separated vortices were observed at low Re. The flow separation and wake of the NACA0012 at low Re were researched in the experiment by Kim et al. (2009). This effect shows that laminar separation in the boundary layer begins to occur when α=3°.Under the condition of Re=4.8×10^4 and α=6°, the reattachment of the airflow is clearly observed, forming the long separated vortex during this process. The impression of the synthetic jet actuator on NACA0022 boundary layer separation and reattachment was studied by Goodfellow et al. (2010), and boundary layer reattachment was enhanced. In the research of Han et al. (2021), the VIV of NACA0012 at high attack angles was investigated. On account of displayed that under different conditions, the unsteady vortex shedding was the same, increasing with increasing speed. Figure 1 shows the flow separation under static angle of attack at different angles. Figure 2 shows the different cases of flow separation for different Re and angles attack.

Fig. 1 Streamlines of average velocity field with NACA0012 attack angle less than 20° (Kurtulus, 2015)

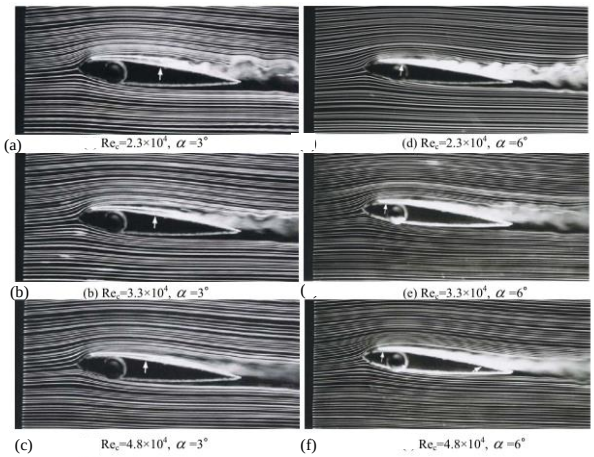

Fig. 2 Boundary layer of NACA0012 at a certain angle of attack and Re (Kim et al., 2009)

The influence of the evolution of the shear layer formed by flow separation on the coherent structure characteristics was inquired by Yarusevych et al. (2009). It was concluded that vortices were created in the shear layer formed by flow separation, and these constructions had an important effect on the modulation from flowing to turbulence. The influence of pitching on the aerodynamic characteristics and flow field situation at a low Reynolds number was tested and investigated by Kim and Chang (2014). The results showed that the first and second tail vortices and mushroom structures depended on the Reynolds number. According to lift and drag coefficient, the hysteresis loop varied with Re. The phase angle of the shear layer formed by flow separation was inversely proportional to the increase of Re. The impression of the attack angle on the vortex structure was studied by Kurtulus (2019). The influence of front hole suction and rear hole blowing on the airfoil has been explored by Zhang et al. (2020), which could suppress disturbances in the flow field. In the case of large-scale heating, vortex shedding is suppressed when the fluid flows through a square column as researched by Arif & Hasan (2019b). It was concluded that large-scale heating played a role in suppressing vortex detachment. Arif & Hasan (2020) simulated the heating and rotation of the cylinder at Re=100. The research results showed that the drag at the same temperature increases along with inclination, while the drag at the same inclination increases along with temperature. Khan et al. (2023) investigated the vortex-induced vibration of mixed convection passing through a cylinder at Re=100. They studied vortices under different conditions and conducted a detailed analysis of the results. The instantaneous vorticity distribution of NACA0012 is obtained when the Reynolds number is Re=1×10^4(t=100s). Lou et al. (2019), Yen and Hsu (2007), Shan et al. (2008), and Nedić and Vassilicos (2015) introduced in detail the effects of low-frequency membrane local vibration, the wing with sweep, vorticity generator, and serrated wing on flow separation. It was deduced that this approach can effectively improve the flow structure. Figure 3 shows the instantaneous vorticity distribution of NACA0012 at Re=1×104 for t=100s.

The synthetic jet actuator could provide high speed and high-momentum jet without a net change of fluid mass in the cavity. The zero-mass jet generated by the actuator disturbs the external flow. The vortex behavior and lift of the airflow are changed by influencing the flow behavior

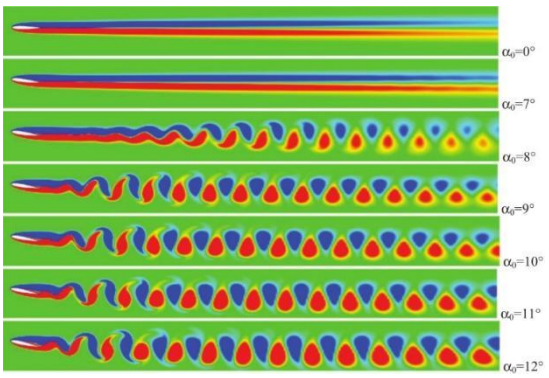

Fig. 3 Instantaneous vorticity distribution of NACA0012 at Re=1×104 (t=100s) (Kurtulus, 2019)

of the airflow. The view that synthetic jets have a pronounced effect on inhibiting flow separation has been verified (You & Moin, 2008; Cao et al., 2020; Wang & Wu, 2020, Kim et al., 2022).

Arif & Hasan (2021) studied the shedding vortex passing through a square column at Re=100. The impression of thermal buoyancy on the aerodynamic characteristics of a square cylinder was obtained. The impression of synthetic jets on the behavior of separated vortices was inquired by Lei et al. (2020). The solution indicated that flow separation was effectively suppressed. The control of large-scale separated flow through synthetic jets has been studied by Tang et al. (2018). It was concluded that synthetic jets were an effective tool for suppressing flow separation and cross-border motion within the separation zone. The method of enhancing the aerodynamic characteristics of airfoils by changing the frequency and momentum of synthetic jets was obtained by Itsariyapinyo and Sharma (2016). The optimization of airfoil parameters using synthetic jets by changing pulse frequency, momentum coefficient, and jet inclination angle was studied by Couto and Bergada (2022). The impression of the jet frequency, angle, and speed on the maximum lift was studied by Neve et al. (2017). The outcome demonstrated that the synthetic jet parameters could enhance maximum lift.

The phase evolution of the separation boundary layer controlled by a synthetic jet for delayed separation was investigated through an experiment by Yang et al. (2022). The outcome displayed that the frequency and amplitude of the synthetic jet significantly affected the reaction of the average shear layer. The increase in the frequency or amplitude of the synthetic jet would increase the length of the reattachment flow. The method of changing the vortex structure by synthetic jet was explored by Wang and Tang (2018) to promote the aerodynamic performance of the airfoil. As a result, the force generated by vortices plays an important role in the performance of airfoils. The synthetic jet could actually postpone or advance the shedding of the leading edge vortex and effectively reduce remove the production of the trailing edge vortex. Thus, the aerodynamic performance and flow separation phenomenon was advanced. The mutual effect between the synthetic jet setting on NACA0012 and the flow field was experimentally studied by Monastero et al. (2019). The constitution and downstream flow of annular flow structures generated by synthetic jets were investigated. This improved the aerodynamic performance of the wing. Arif & Haasan (2019a) studied mixed convection in a heated square column with Re=100. He investigated the effects of using different characteristic numerical boundary conditions when solving using non-Boussinesq methods.

The mutual effect between the array jet and the airfoil flow field was experimentally researched by Lindstrom et al. (2018). Conclusion drawn the separation flow on the controlled surface of the synthetic jet was reattached. The synthetic jet active control to the flow separation control of a vertical tail was experimentally investigated by Monastero and Amitay (2016). The outcome displayed that the synthetic jet control substantially changed the

global pressure distribution around the model. The impression of jet breadth and amplitude on the flow above the NACA0012 was explored by Saadi and Bahi (2018). The lift drag ratio would change as the width of the jet changes. The direct simulation results of the jet on the NACA0018 were presented by Zhang and Samtaney (2015). It showed that the synthetic jet has a significant impact on the vortex structure. The outcome of jet excitation frequency on airfoil airflow was investigated through an experiment by Feero et al. (2015). The consequence indicated that the high frequency could eliminate the massive vortex shedding in the wake. According to Singh et al. (2021) and Tadjfar & Kamari (2020), the vortex structure and lift could be changed by employing a jet array or placing the jet at the tail end of the vertical wing. According to Feero et al. (2017) and Moshfeghi and Hur (2017), the vortex structure and lift can be changed by changing the width, injection angle, blowing ratio, and the position of synthetic jet.

The synthetic jet with fixed frequency or combined frequency had a meaningful impression on the vortex and flow field near the surface. But the mechanism is not clear. At present, the impression of jet frequency on airfoil vortex structure and lift has been investigated from multiple perspectives. This research simulates the flow of synthetic jets under different attack angles, discussing the laws of vortex structure evolution. In-depth study of the vortex discharge rate on the aft edge with changes in lifting force and resistance coefficient. Be aim of this paper is to inquire about the outcome of the excitation frequency of jets on the vortex structure and aerodynamic parameters near the wing surface.

2. PHYSICAL MODEL AND NUMERICAL SIMULATION METHOD

2.1 Physical Model

In this paper, the computational domain model refers to the computational domain structure by Chang et al. (2022). Detailed parameters are as follows. Wing characteristic length is set to 0.1 m. The interval from the left of the airfoil to the leading edge, the right to the tail edge, and the top and bottom to the wing chord are all 1.5 m. A non-structured mesh is used in the airfoil. There are 138490 grids. The initial height of the boundary layer is obtained according to the incoming Mach number and the characteristic length. The value of Y+ is 1. The inlet of air is velocity inlet, the wall surface and wing surface are non-slip walls, and the outlet is pressure outlet. The geometric model size is large enough relative to the wing size, so the range from airflow entering the flow field to flow separation and full development of wake can be included. The impression of the boundary of the calculative domain on the flow field simulation is avoided. The computational domain and meshing are shown in Fig. 4 and Fig. 5

After research, it was discovered that installing the synthetic jet in front of the flow separation point has a better influence than after (Goodarzi et al., 2012). With the attack angle increasing, the separation point of the upper airflow surface is moved forward. After analysis, the synthetic jet actuator will be arranged as follows: the α is set to 10°, 14°, and 16° when the actuator position is at

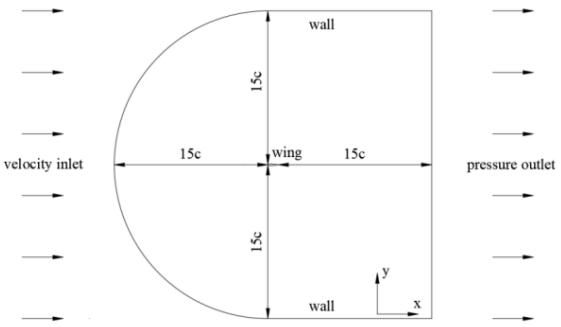

Fig. 4 NACA0012 airfoil calculation domain and conditions

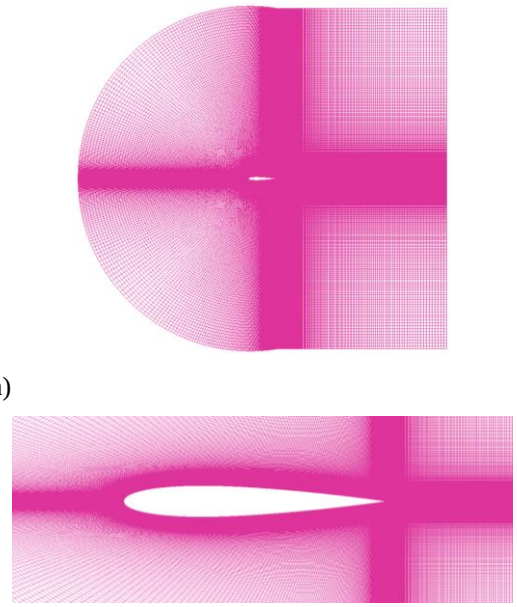

(a)

(b)

Fig. 5 NACA0012 airfoil calculation grid (a) global grid (b) grid around the airfoil

7.6% chord length, and the α is set to 19° and 22° when it is at 1%. The width of the jet port is 1% of the characteristic Length. The blowing and suction frequency of the jet conforms to the fluctuation law of the sine function, as shown in Eq. 1.

$$V=2\pi ft \tag{1}$$

2.2 Flow Control Equation

The governing equations of the fluid include the conservation of mass (continuity), the conservation of momentum (N-S), and energy conservation.

The conservation of mass can be explained as:

$$\frac{\partial \rho}{\partial t}+\frac{\partial(\rho u_x)}{\partial x}+\frac{\partial(\rho u_y)}{\partial y}+\frac{\partial(\rho u_z)}{\partial z}=0 \tag{2}$$

the ρ, t, and u are density, flow time, and flow velocity vectors, respectively, and u_x, u_y, and u_z are the XYZ direction component of the velocity vector along the global coordinate system, and the lower corner represents different directions.

$$\begin{cases} \frac{\partial u}{\partial t} + (u \cdot \nabla)u = f - \frac{1}{\rho}\nabla P + \nu \nabla^2 u \\ \nabla \cdot u = 0 \end{cases} \quad (3)$$

The above is the N-S equation corresponding to the incompressible fluid solved in the paper:

where f, ∇P, and v are respectively mass force, pressure gradient, and kinematic viscosity of the fluid .

The energy conservation is one of the basic governing equations of fluid flow. The flow field condition calculated in this paper is incompressible flow, in which the heat exchange has rarely impression on the fluid calculation. Therefore, the effect of the energy equation is not considered in the simulation.

2.3 Turbulence Model

Turbulence occurs due to changes in velocity. Momentum, energy, and concentration are caused by velocity fluctuations in a fluid medium and cause fluctuations in quantity. Due to the small scale and high frequency of this fluctuation, direct simulation requires high requirements for computers. In fact, the transient control equation may be uniform in time and space, or the scale of the transient control equation can be artificially changed, requiring less equation modification.

According to the Boussinesq hypothesis, the Reynolds averaged Navier-Stokes equation (RANS) is closed using a turbulence model. The model was selected as the standard k-omega model. The model is an empirical model based on turbulent kinetic energy (k) and dissipation rate (ω). This turbulence model is used to calculate the fluid velocity in the viscous sublayer near the wall with good convergence. However, the k-ω model performs well in the characteristic of the reverse pressure gradient boundary layer, the wall-bounded and low Reynolds number turbulence, and the large turbulent simulation. The calculation expression of the turbulence coefficient is:

$$\begin{cases} \rho \frac{dk}{dt} = \frac{\partial}{\partial x_i}\left[\left(\mu + \frac{\mu_t}{\sigma_k}\right)\frac{\partial k}{\partial x_i}\right] + G_k + G_b - \rho\varepsilon - Y_M \\ \rho \frac{d\varepsilon}{dt} = \frac{\partial}{\partial x_i}\left[\left(\mu + \frac{\mu_t}{\sigma_\varepsilon}\right)\frac{\partial \varepsilon}{\partial x_i}\right] + G_{1\varepsilon}\frac{\varepsilon}{k}(G_k + C_{3\varepsilon}G_b) - G_{2\varepsilon}\rho\frac{\varepsilon^2}{k} \end{cases} \quad (4)$$

Where G_k represents turbulence energy from the average speed gradient, G_b stands for turbulent kinetic energy caused by lift force, Y_M is the impression of compressible pulsation of turbulence on the overall dissipation, and u_t is the coefficient of viscosity of turbulence. The solution for u_t is:

$$\mu_t = \alpha * \frac{\rho k}{\omega} \quad (5)$$

2.4 Grid Independence Verification

Figure 6 shows the curve for different grid numbers at the same angle. When the number of grids is small, the resulting error is relatively large, while adding a grid number will lead to a close number of results. So as to promise the exactitude of numerical simulation, save resources, and accurately obtain the flow characteristics in the flow field calculation domain, a model with a grid number of about 130000 should be selected for numerical simulation. The maximum error is not more than 5%, and

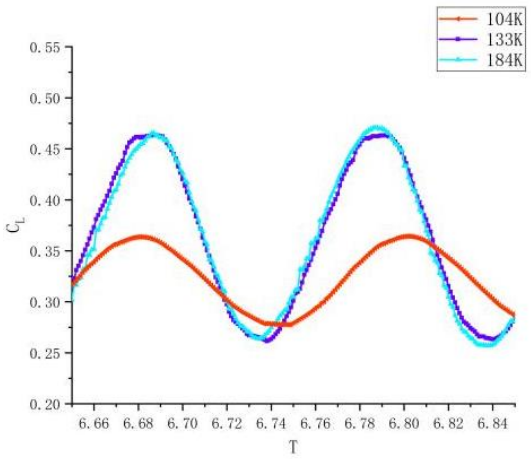

Fig. 6 Coefficient curve for different grid numbers and the same attack angle

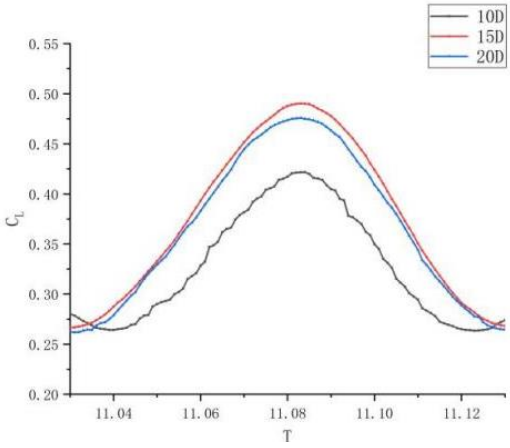

Fig. 7 Regional independence verification

we can assume that the calculation results in the manuscript are appropriate.

2.5 Domain Independence Verification

Figure 7 shows the lift coefficient curves under the same grid drawing method in the 10D, 15D, and 20D regions. From the images, it can be seen that the data obtained in the 15D region is consistent with that obtained in the 20D region, but the 10D region had a obvious difference in the data. It can be seen that the results differ significantly when the region is small compared to that when the region is large, while increasing the region will lead to close results. So as to guarantee the precise of numerical simulation, save resources, and accurately obtain the simulation consequence, a model with a grid area of about 15D should be selected for numerical simulation. The maximum error is less than 3%, and we can assume that the calculation results can be accepted.

2.6 Accuracy Verification

So as to verify that the flow field model can resultful simulate the research content of this article, the model construction method used in this article was utilized to construct a physical model under the same conditions as Shen et al. (2017) and Di Ilio et al. (2018), and numerical

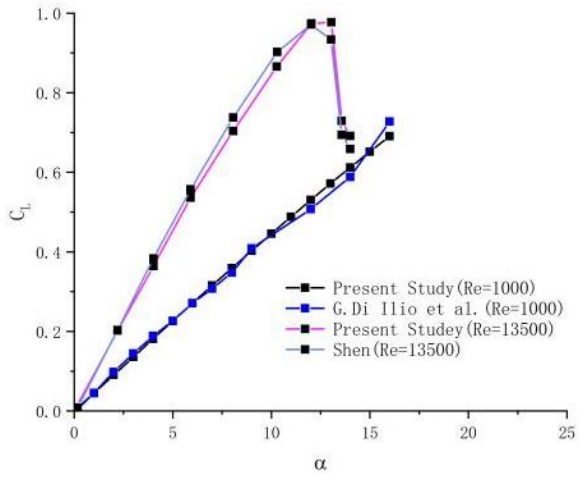

Fig. 8 Comparison of lift coefficient

simulations were used to compare the simulation results with the conclusions of Shen et al. (2017) and Di Ilio et al. (2018). The comparison results are shown in Fig. 8. When other conditions are the same as the reference, the research is the lifting force coefficient calculated by the standard k-omega model, which is better suited to the results of digital simulations in literature. Although the attack angle where the maximum lift coefficient occurs deviates from the attack angle in the reference, the maximum error is still less than 5%. The lift curve still accurately response to the change of the airfoil stall concerning the attack angle.

3. RESULTS AND DISCUSSION

The characteristic parameters of a synthetic jet include excitation waveform, excitation frequency, excitation amplitude, excitation phase, etc. The change of the above parameters directly affects the working performance of the actuator. As a result, the jet affects the impression of controlling the vortex structure on the absorption surface. Vortex structure has an important influence on pneumatic profile parameters. The impression of the jet whose excitation frequency is investigated in this paper below.

In flow control of synthetic jet, there is no mechanical motion structure in the exciter of synthetic jet, and the environmental fluid is periodically blown and pumped, driven by the excitation voltage, which conforms to zero-mass jet characteristics. The working mechanism of a synthetic jet actuator is a discontinuous jet generated by blowing and sucking the surrounding fluid. Thus, the fluid of the exciter cavity and the external environment exchange passively periodically. For a given size actuator, the control impression of the jet is obviously related to the excitation frequency.

3.1 Analysis of Wing Vortex Shedding Under Fixed Excited Frequency Synthetic Jet

In Chang et al. (2022), the structure and frequency characteristics of NACA0012 airfoil shedding vortex under a specific flow field environment are analyzed, and flow patterns in the range of 0° to 24° attack angles are briefly described. Different flow forms correspond to different spectral characteristics of the frequency plot of the rising resistance coefficient. The highest frequency of amplitude in the range of amplitude lifting power indicates that the vortex below this frequency contains the highest energy. The theory of the jet is to transform the structure of the flow field and improve aerodynamic performance by creating a discontinuous jet by blowing and absorbing the surrounding fluid. And in the blowing and suction process, vortexes are generated near the excitation port. When the frequency of the vortex generated is similar to the wing airfoil, the flow around the wing airfoil is "locked". At this time, the excitation effect is obviously better than that under other fixed frequencies (Wu et al., 1998).

Table 1 Excitation function of synthetic jet with fixed excitation frequency

Angle of attack	Expression of excitation function of synthetic jet	Duration of blowing and suction cycle
$\alpha = 10°$	$\sin(2\pi * 18.67 * t)$	0.05 s
$\alpha = 14°$	$\sin(2\pi * 11 * t)$	0.09 s
$\alpha = 16°$	$\sin(2\pi * 10.33 * t)$	0.1 s
$\alpha = 19°$	$\sin(2\pi * 6.67 * t)$	0.15 s
$\alpha = 22°$	$\sin(2\pi * 6 * t)$	0.17 s

Based on the content in Chang et al. (2022), the study of this research, the impression of the frequency of jet on the drag to airfoil lift by five attack angles. The excitation function of the synthetic jet is as in Table 1.

NACA0012 vorticity diagram and flow diagram are shown in Fig.9~13, which is under the excitation of a synthetic jet with Re =10^4. Q criterion is adopted as the evaluation criterion of the vorticity diagram, among them, q >0 means that the vortex plays an important role, and q <0 means that the no vortex plays an important role.

As shown in Fig. 9, The fluid is periodically blown and sucked in by the actuator port α=10°and f=18.67 Hz. Compared with the vortex is structured in the field of α=10° in Chang et al. (2022), the amount of vortex structures on the upper surface, as the active excitation of the jet increases. When t=1/2T, it is a blowing process. At this time, the main vortex structures on the upper surface include the resident vortex (marked as D1), the first shedding vortex (D3), and the second shedding vortex (D5). The counterclockwise secondary vortex D2 is generated between the clockwise vortex D1 and D3. In the same way, the counterclockwise secondary vortex D4 is formed between D3 and D5.

Figure 10 illustrates that when α=14° and f=11 Hz, the shedding wake vortex presents a periodic vortex street form. The time from 1/5T (Fig. 10 (a, b)) to 2/5T (Fig. 10 (c, d)) is the synthetic jet-blowing process. The time from 3/5T (Fig. 10 (e, f)) to 5/5T (Fig. 10 (i, j)) is the suction process of a synthetic jet.

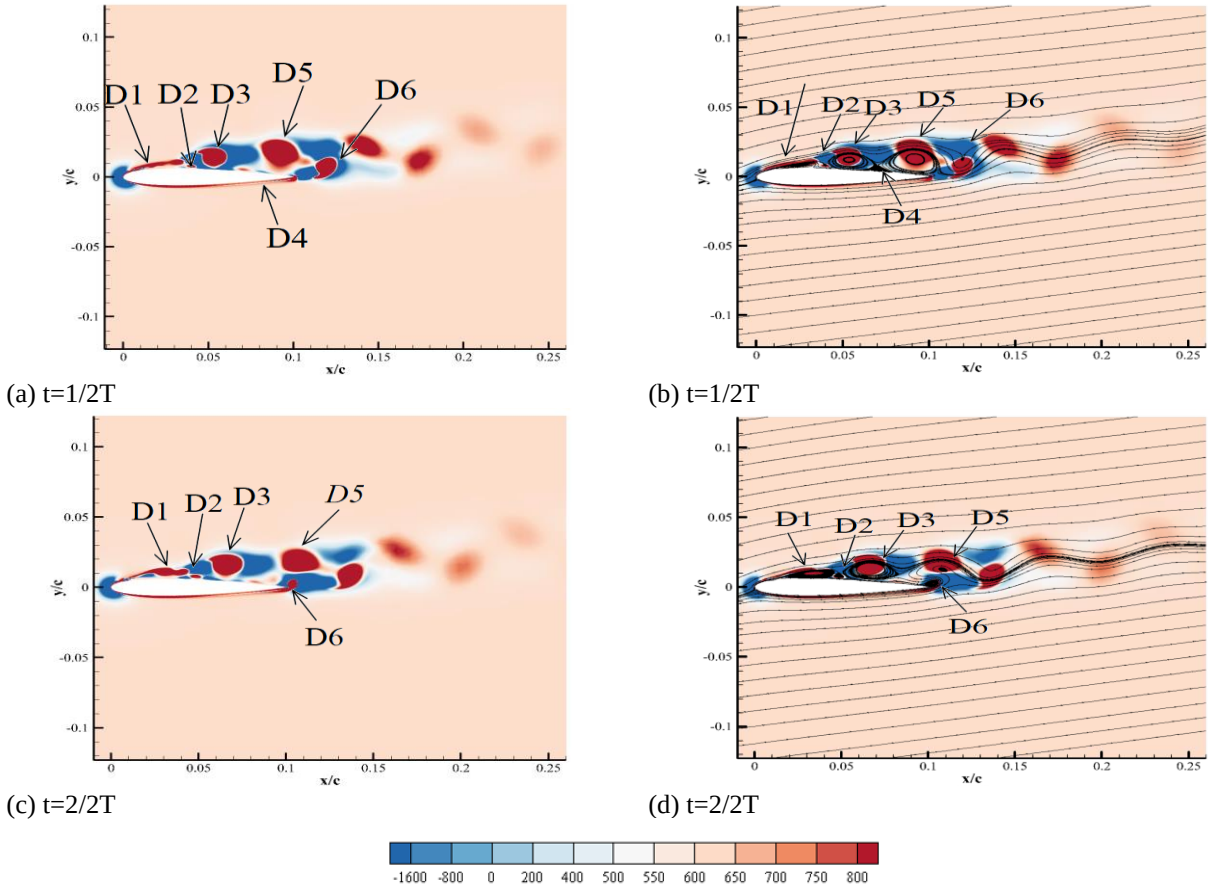

Fig. 9 Periodic vorticity diagram and streamline diagram of shedding vortex when the excitation frequency is f=18.67 Hz, α=10 ° attack angle (In the vorticity diagram, the red indicates that vorticity is dominant, and the blue indicates that viscous stress is dominant)

When *t*=1/5T (Fig. 10 (a, b)), the vortex E1 is generated by the fluid blowing from the actuator mouth at 7.6% of the chord length. The separation vortex system of the upper surface begins to develop from the separation vortex formed at the end of the previous cycle. The structure of the wing-type separation vortex system is as follows. Standing vortex E2, secondary vortex E3, shedding vortex E4, and airfoil pressure surface entrainment vortex E5.

When the time is 2/5T (Fig. 10 (c, d)), the actuator continuously blows fluid and injects energy into the vortex E1, and the vortex E1 moves backward under the impression of the incoming flow. The upper surface will separate at a certain chord length under the dual action of viscosity and reverse pressure gradient. At this time, the kinetic energy of the incoming flow can not offset the blocking effect of the above reasons. Obstruction causes the incoming flow to leave away from the airfoil surface, causing flow separation. When α=14°, the actuator is located in front of the separation point of the upper surface. Compared with that without a synthetic jet, the kinetic energy of incoming flow at the separation point is increased by vortex E1, which improves the ability of incoming flow to resist flow separation. The synthetic jet actuator moves the boundary layer flow separation point towards the trailing edge, delaying the separation position.

According to Fig. 10, from *t*=1/5T to *t*=2/5T, the vortex E1 gradually increases in size. The size of vortex E1 is proportional to the amount of accumulated energy. At this time, the E5 vortex falls to the upper surface and gradually disappears. Because of the action of incoming flow, the resident vortex E2 and secondary vortex E3 move toward the back edge of the airfoil. The entrainment vortex E5 accumulates energy and is close to falling off.

The jet is in the suction process at the time 3/5T (Fig. 10 (e, f)). There is no vortex generated near the excitation port. The flow before the separation point of the airfoil is approaching the airfoil surface because of the suction process. At this time, a new shedding vortex (marked as E6 and E7) is formed by the resident vortex E2 and merges with the secondary vortex E3. Simultaneously, the entrainment vortex E5 is about to fall off.

At the time 4/5T (Fig. 10 (g, h)), a new shedding vortex E10 is generated by merging vortex E6 and vortex E7. The flow separation in the front edge of the airfoil makes the persistent vortex E8 generated. The secondary vortex E9 emerged under the double action of vortex E8 and E10. The entrainment vortex E5 falls off simultaneously.

The synthetic jet actuator will change from the suction process to the blowing process when t=5/5T (Fig. 10(i, g)).

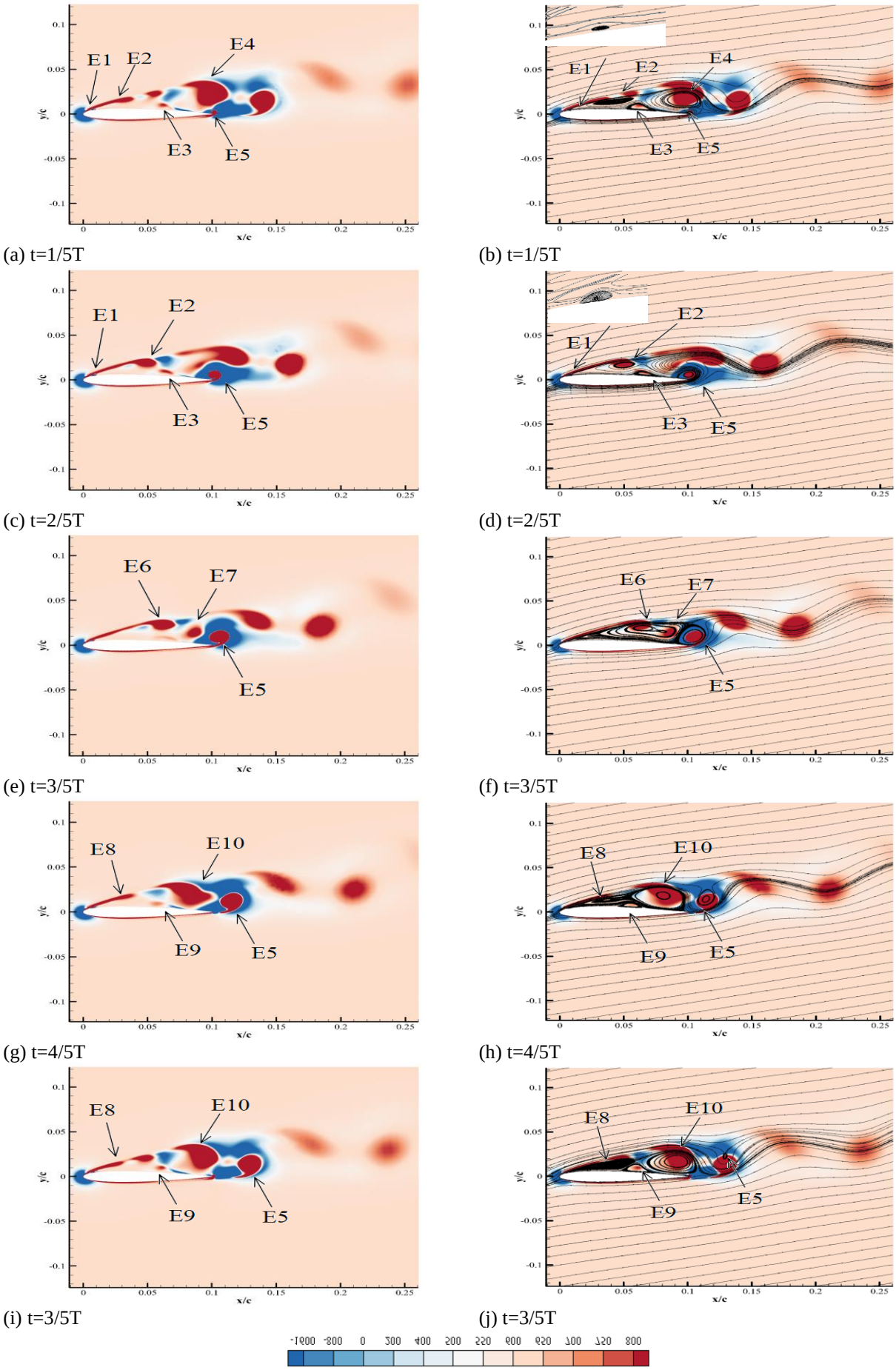

(a) t=1/5T (b) t=1/5T

(c) t=2/5T (d) t=2/5T

(e) t=3/5T (f) t=3/5T

(g) t=4/5T (h) t=4/5T

(i) t=3/5T (j) t=3/5T

Fig. 10 Periodic vorticity diagram and streamline diagram of shedding Vortex at α=14° and f=11 Hz

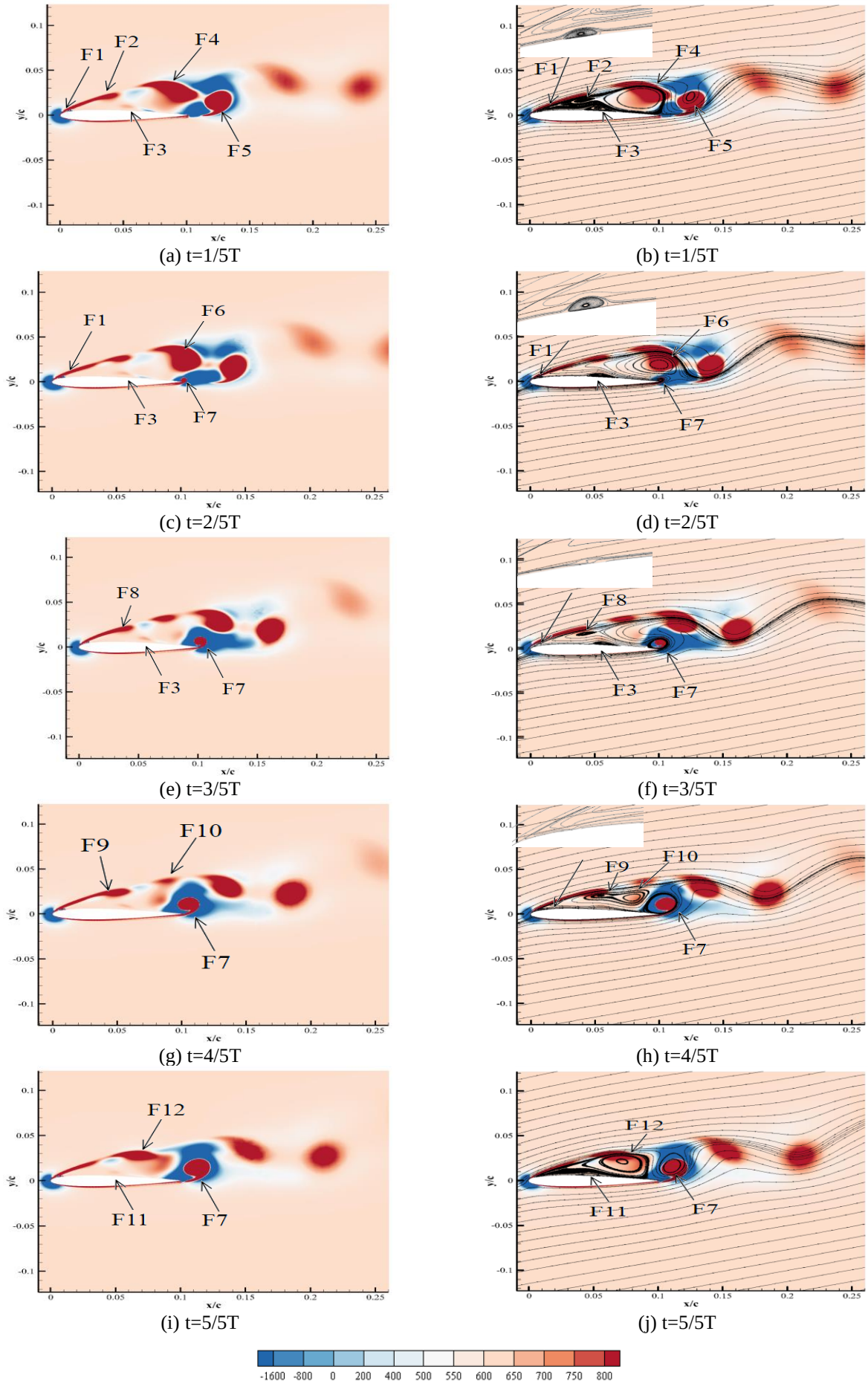

(a) t=1/5T (b) t=1/5T

(c) t=2/5T (d) t=2/5T

(e) t=3/5T (f) t=3/5T

(g) t=4/5T (h) t=4/5T

(i) t=5/5T (j) t=5/5T

Fig. 11 Periodic vorticity diagram and streamline diagram of shedding Vortex at the α=16° and f=10.33 Hz

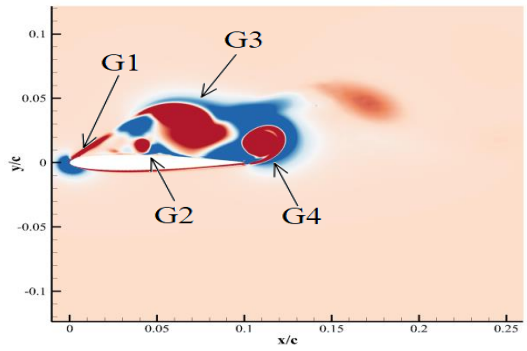

(a) t=1/6T

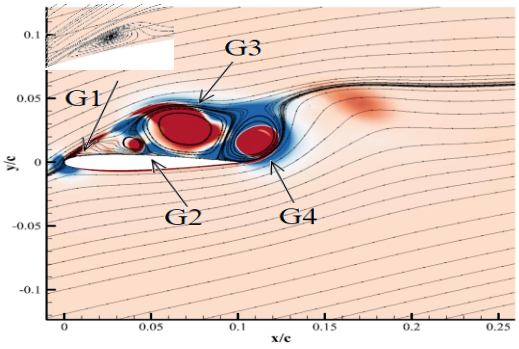

(b) t=1/6T

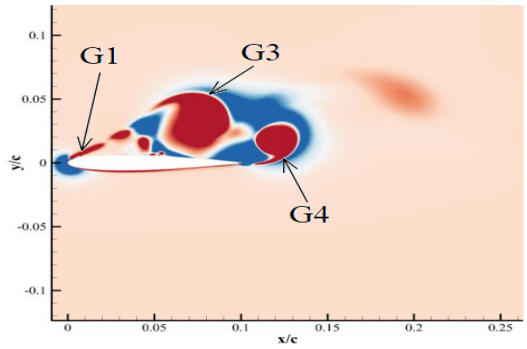

(c) t=2/6T

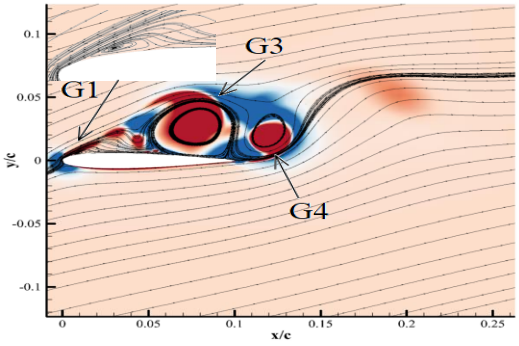

(d) t=2/6T

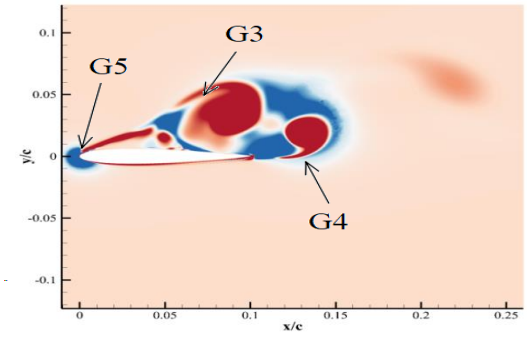

(e) t=3/6T

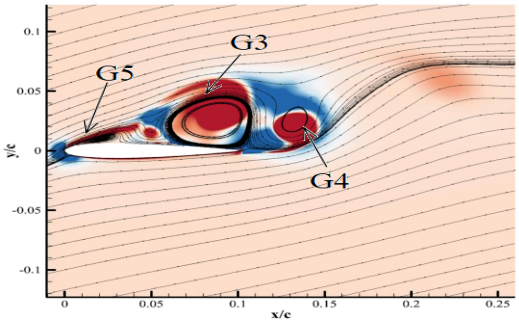

(f) t=3/6T

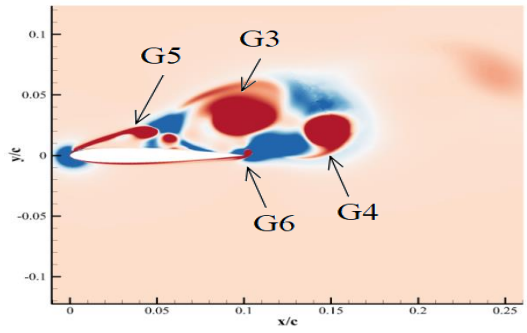

(g) t=4/6T

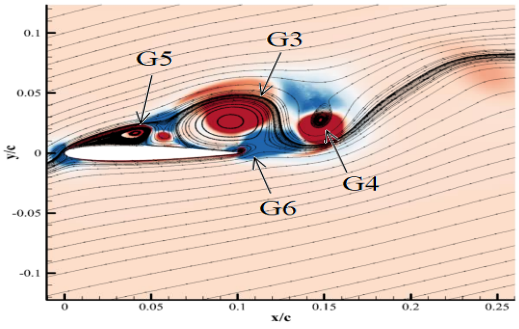

(h) t=4/6T

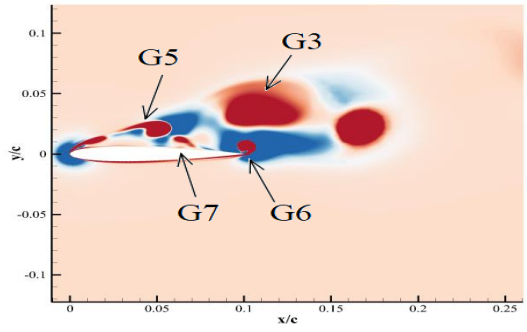

(i) t=5/6T

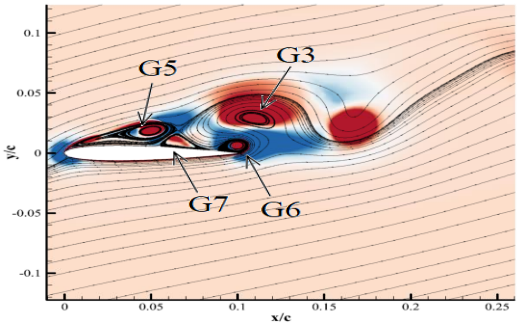

(j) t=5/6T

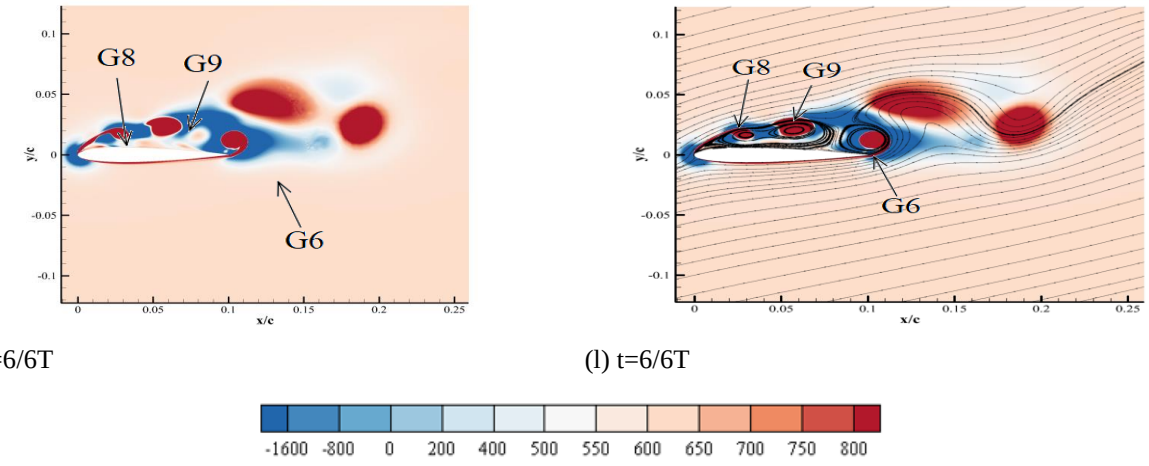

(k) t=6/6T (l) t=6/6T

Fig. 12 Periodic vorticity diagram and streamline diagram of abscission vortex when *f*=6.667 Hz and *α*=19°

The wing suction plane vortex is the same as the previous one. The entrainment of vortex E5 further consumes energy in the wake and is about to dissipate. The above process is a complete shedding vortex cycle under the *α*=14° and the *f* = 11 Hz.

As shown in Fig. 11, the structure at *α*=16° and *f*=10.33 Hz is similar to that at *α*=14° and f=11 Hz. As depicted in Fig. 11(a, b), when *t*=1/5T, the vortex system structure above the wing is excitation vortex F1, resident vortex F2, secondary vortex F3, Shed vortex F4 and entrainment vortex F5. During the suction process, the vortical structure current structure is also similar to that at *α*=14°. At *t*=3/5T, the standing vortex F8 at the leading edge gradually transits to the shedding vortex F9 at *t*=4/5T. Under the double action of vortex F9 and trailing edge entrainment vortex F7, the shedding vortex F10 is generated. When *t*=5/5T, vortex F9 and F10 merge to generate the shedding vortex F12.

Figure 12 is the process of shedding vortex when *α*=19° and *f*=10.33 Hz. In the Fig. 12(a, b), the vortex structure of the upper surface in the process of the jet-blowing process is jet excitation vortex G1, secondary vortex G2, detached vortex G3, entrained vortex G4. And there is no resident vortex. Under the action of G1, part of the fluid in front of the edge of the airfoil is close to the airfoil. At this time, the jet actuator remains in front of the flow separation point and is located at 1% of the characteristic length. As the jet continues to blow out, when *t*=2/6T (Fig. 12 (c, d)), vortex G1 drives the fluid approaching the wing, and vortex G2 is impacted into the surrounding flow field and detached vortex G3.

At *t*=3/6T, the synthetic jet actuator changes from the blowing process to the suction process, and the leading edge resident vortex G5 starts to generate. At *t*=5/6T, the entrainment vortex G4 has dissipated in the wake. The new entrainment vortex G6 is accumulating energy. Under the action of vortex G5 and G6, the secondary vortex G7 appears. Vortex G5 and G7 merge to generate a new shedding vortex G9 when *t*=6/6T. A new resident vortex, G8, emerges at the leading edge.

According to Fig 13, the shedding wake still presents a periodic vortex street form when *α*=22° and *f*=6 Hz. Because as the angle gets larger, the change in the structure of synthetic jet is not much, and the generated jet vortex will quickly merge into the airfoil leading edge resident vortex (marked as vortex H1 in Fig. 13). The vortex structure includes the resident vortex H1, the secondary vortex H2, the shedding vortex H3, and the entrainment vortex H4.

From *t*=1/6T to *t*=3/6T, the actuator is the blowing process. At this time, the leading edge resident vortex H1 and secondary vortex H2 stably exist at the front chord length of the airfoil. From *t*=4/6T to *t*=6/6T, the actuator is in the suction process. At this time, the standing vortex H1 in front of the edge gradually disappears, and the vortex structure is composed of the secondary vortex H7 and the shedding vortex H8. The above process is a complete shedding period of the vortex at *α*=22° and *f*=6 Hz.

3.2 Analysis of Frequency Characteristics of Shedding Vortex under the Action of Synthetic Jet with Fixed Excitation Frequency

The control of airfoil vortex lift can be achieved by capturing the vortex structure through low-power periodic excitation. The control effect of periodic excitation is better than that of constant excitation. The physical mechanism of the low-power synthetic jet controlling the airfoil lift is: (1) the periodic vortex structure appears above the wing changes, (2) the excited vortex is used to actively control the flow field, (3) a response is produced by the vortex structure above the wing changes, (4) the lift coefficient is changed by the vortex structure.

Table 2 Root mean square coefficients of airfoil lift and drag for a single frequency synthetic jet exciter

Angle	Frequency	Lift (RMS)	Resistance (RMS)
10°	sin(2π*18.67*t)	0.5285	0.1375
14°	sin(2π*11*t)	0.7322	0.2477
16°	sin(2π*10.33*t)	0.8411	0.3057
19°	sin(2π*6.67*t)	1.0050	0.4252
22°	sin(2π*6*t)	1.0296	0.5094

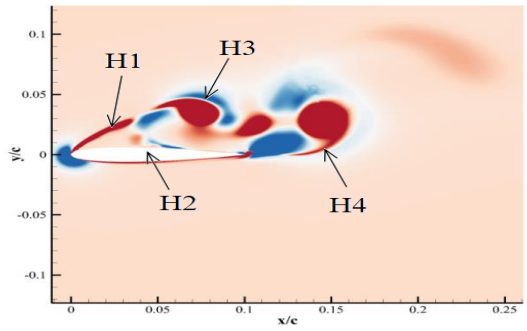

(a) t=1/6T

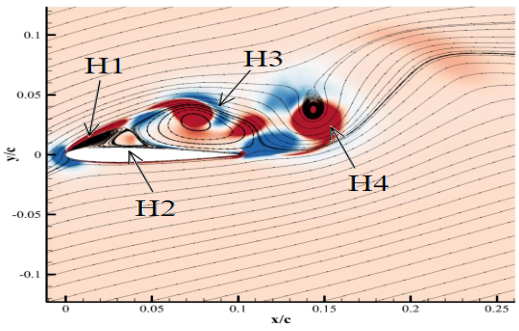

(b) t=1/6T

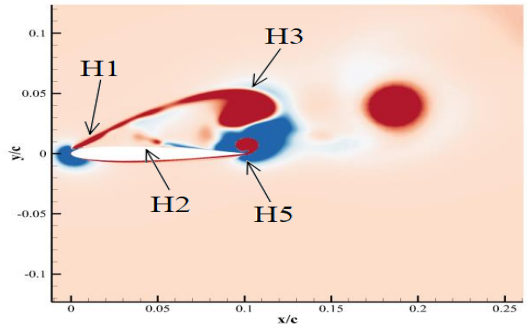

(c) t=2/6T

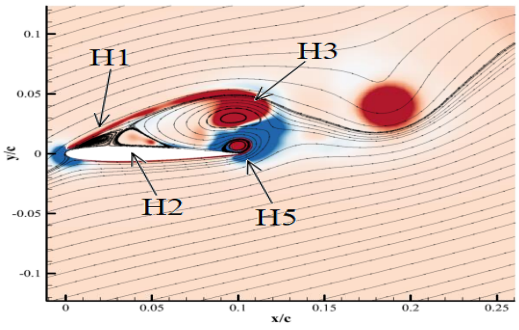

(d) t=2/6T

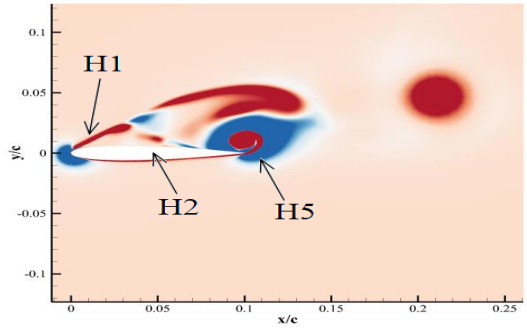

(e) t=3/6T

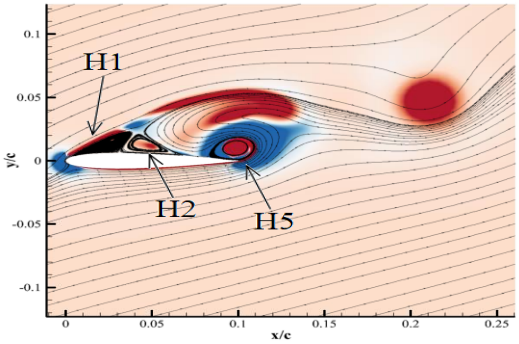

(f) t=3/6T

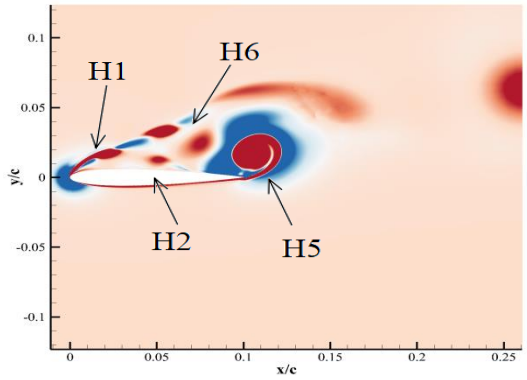

(g) t=4/6T

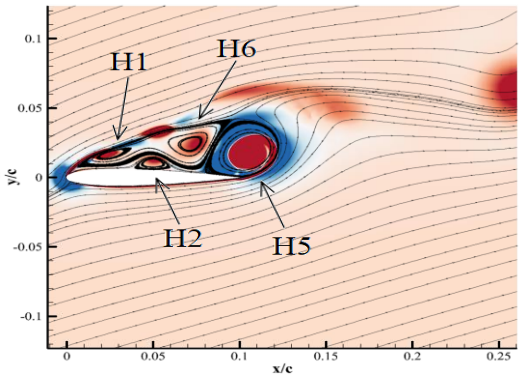

(h) t=4/6T

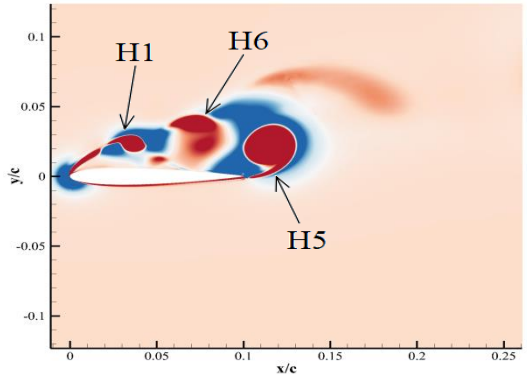

(i) t=5/6T

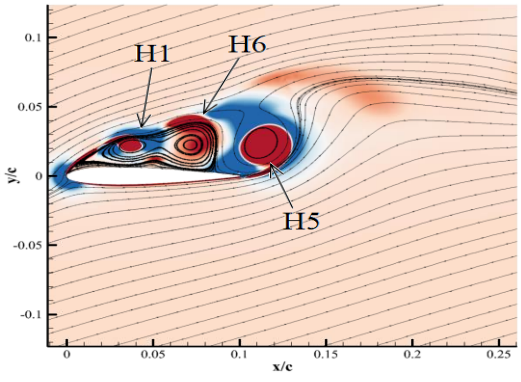

(j) t=5/6T

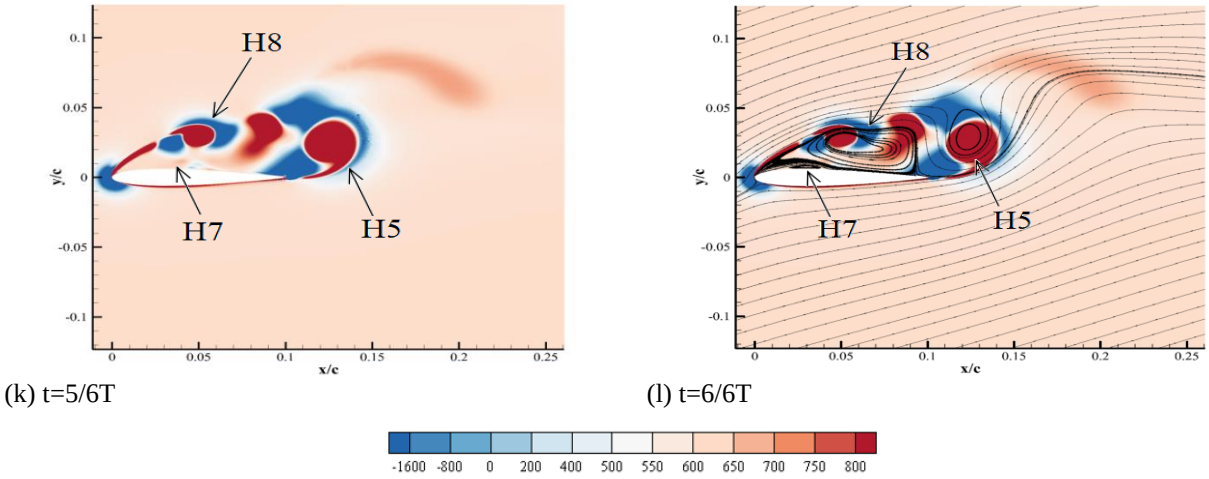

(k) t=5/6T (l) t=6/6T

Fig. 13 Vorticity diagram and streamline diagram of shedding vortex period when f=6 Hz and α=22°

As picture in Fig. 14 (a), the curves of airfoil show sinusoidal vibration. In Fig.14 (b), the spectrum of lift coefficient with α=10° is significantly different between *f*=18.67Hz and that with no excitation. The addition of a jet causes the lift coefficient to change.From the lift coefficient spectrum, it is obvious that it has one main frequency and two harmonic frequencies. The frequency values are respectively 9.67 Hz, 19.67 Hz and 29.34 Hz.

At the condition of α=10°, the vortex structure of the flow field is broken by the synthetic jet. The flow characteristics of the suction surface of an airfoil with multiple vortices coexist. As shown in Fig. 9, the lift increase is due to the incoming flow being driven by vortices through the surface. However, as the vortex itself is a highly viscous energy body, it will increase friction with the airfoil in the process of moving to the back edge of the airfoil under the action of the incoming flow, resulting in an increased drag coefficient. After changing the frequency, the vortex shedding in the flow field also shifts from 2S to quasi-periodic mode. Moreover, the intensity of the main frequency of the separated vortex on the upper surface is increased from 0.0075 to 0.12, compared with that without the synthetic jet. At α=10°, the lift coefficient with a jet is 43% higher than that without a jet actuator.

In Fig.14 (e), it is obvious that the main frequency in the frequency domain diagram is 11.02 Hz at α=14°. In addition, there are two harmonic frequencies: f=22.002 Hz and f=33.03 Hz, respectively. The amplitude of the main frequency increases to approximately 0.15. By comparing Fig. 14 (e) with the result of Chang et al. (2022), only the second harmonic frequency f=33.03 Hz has been added, and the changes in other frequencies are not significant.

As shown in Fig. 14 (d), the drag coefficient has small wave crest fluctuations a comparison between the lift coefficient. This indicates that the change of the vortex structure around the airfoil flow field has a more obvious impression on the drag coefficient than on the lift coefficient. The emergence of new harmonic frequencies indicates a transformation in the vortex structure of the flow field. When the coefficient curves reach the trough, it signifies that the vortex capacity on the lower surface of the wing accumulates to its maximum and is about to fall off. The subsequent rise of these two curves means that the vortex starts to weaken. Similarly, when the curve reaches its peak, it indicates that the vortices on the surface of the wing begin to detach. At α=14°, the strength of the vortices on the lower surface is much greater than that on the upper. Therefore, the two curves do not fluctuate significantly and still conform to the quasi-sinusoidal oscillation. Under the excitation, coefficient curves and vortice conditions of α=14° are similar to α=10°. At this time, the flow field still conforms to the 2S (single). At α=14°, the lift coefficient of the airfoil with a jet actuator is 28.5% higher than that without a jet actuator.

After adding a synthetic jet actuator, according to Fig. 14 (g, h), the curve transitions at α=16° from an unordered state to a sinusoidal periodic curve, as shown in the research of Chang et al (2022). This also indicates the vortex structure changes from chaotic to a 2S-like (Single) mode. In Fig. 14 (h), two values appear, which are the dominant frequency of *f*=9.717 Hz with an amplitude of 0.12 and the harmonic frequency of *f*=19.43 Hz with an amplitude of 0.03.

After applying the synthetic jet, although the flow state of α=16° changes from a chaotic state to quasi 2S (Single) mode, the amplitude of the dominant frequency is lower than that of α=14° and *f*=11.01 Hz. The strength data show that the chaotic state can transform into a quasi-regular state by adding a synthetic jet. However, some energy of the jet vortex is dissipated in the course of breaking the large vortex in the airfoil suction surface vortex system. Therefore, it is obvious that in Fig. 14 (h), the amplitude is only 0.12 when the main frequency is 9.717 Hz, which is equal to the amplitude of α=10°.In general, the lift coefficient of an airfoil with a jet actuator at α=16° is 32% higher than that without a jet actuator.

When α=19°, the addition of an actuator with *f*=33.03 Hz makes the flow state change from 2S mode to quasi-2S mode. According to Fig. 14 (k), there are multiple subharmonic frequencies with equivalent amplitudes, whose amplitude is approximately 0.04. It is obvious that the synthetic jet generates multiple small vortices on the surface. These vortices have different frequencies but similar intensities.

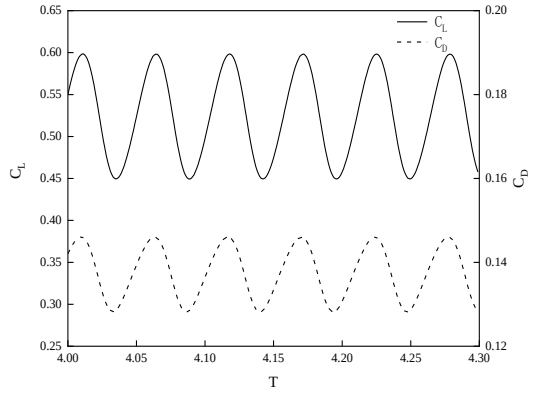

(a) α=10° and f=18.67 Hz

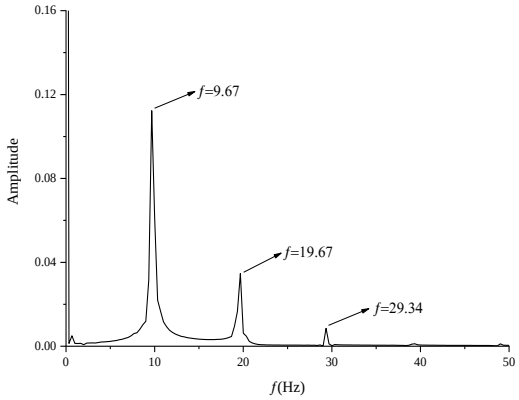

(b) Lift with α=10° and f=18.67 Hz

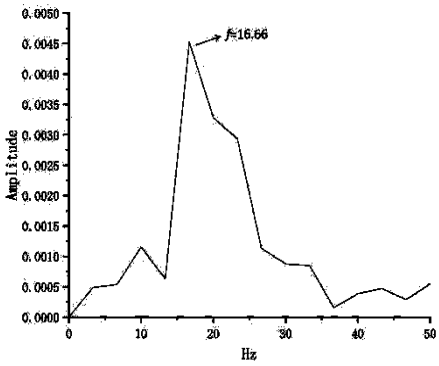

(c) Drag with α=10° and f=18.67 Hz

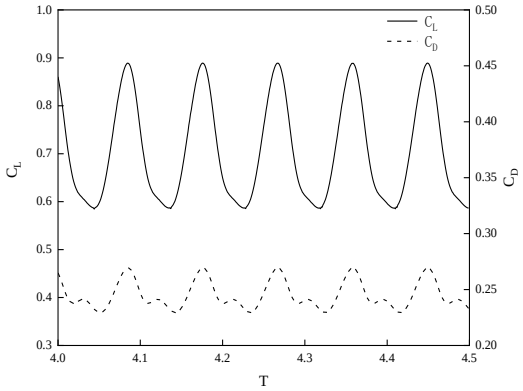

(d) α=14° and f=11.00 Hz

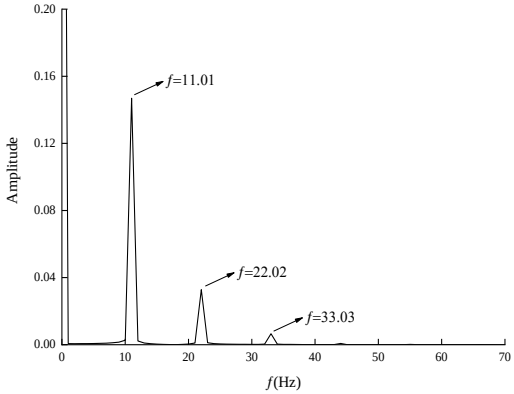

(e) Lift with α=14° and f=11.00 Hz

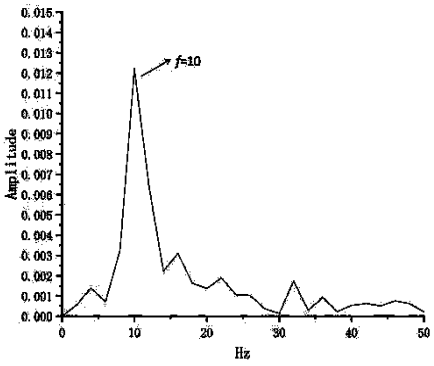

(f) Drag with α=14° and f=11.00 Hz

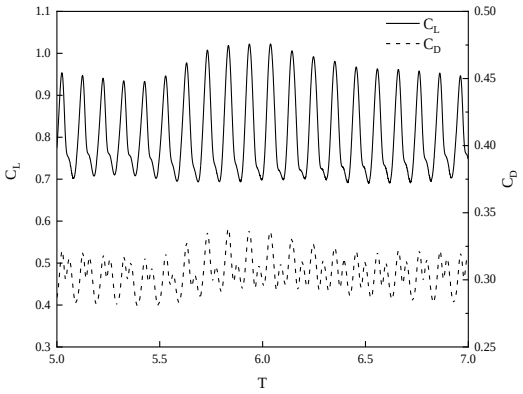

(g) α=16° and f=10.33 Hz

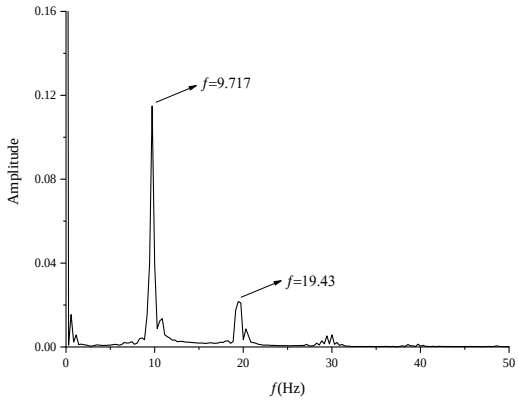

(h) Lift with α=16° and f=10.33 Hz

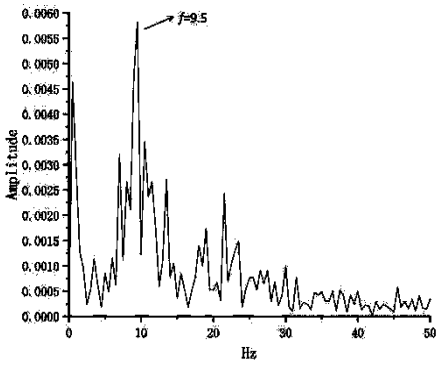

(i) Drag with α=16° and f=10.33 Hz

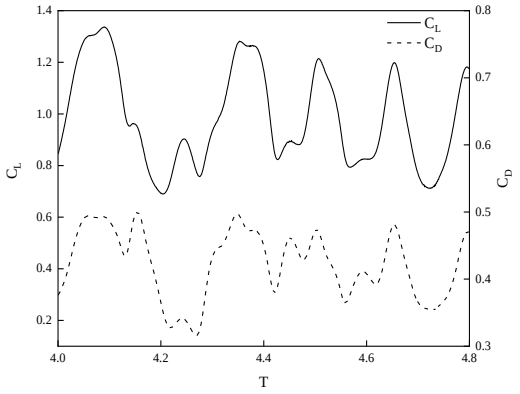

(j) α=19° and f=6.667 Hz

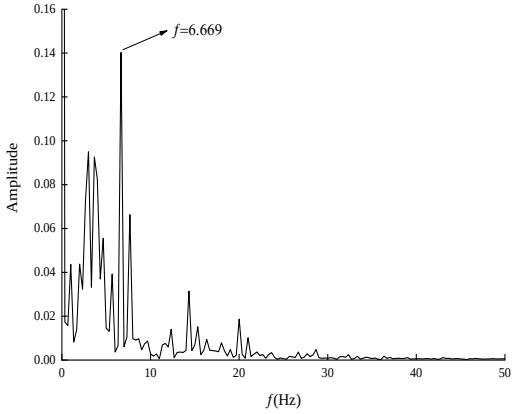

(k) Lift with α=19° and f=6.667 Hz

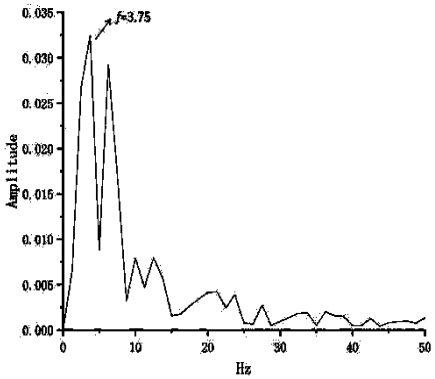

(l) Drag with α=19° and f=6.667 Hz

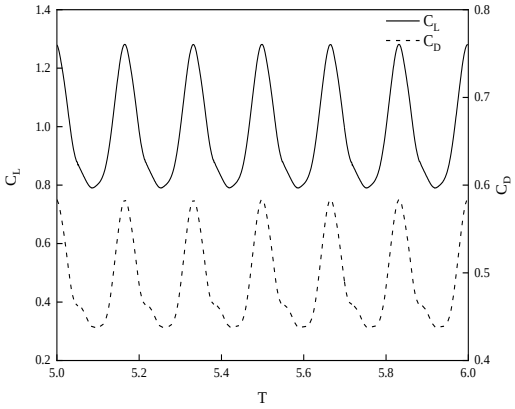

(m) α=22° and f=6.000 Hz

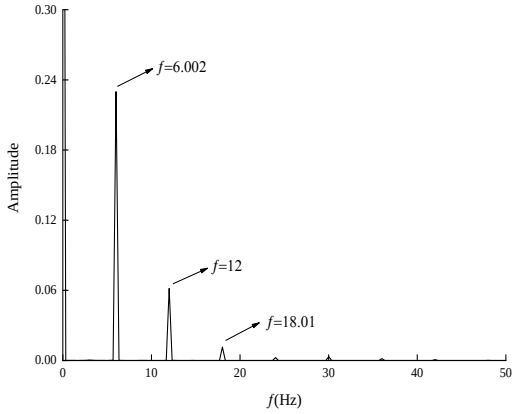

(n) Lift with α=22° and f=6.000 Hz

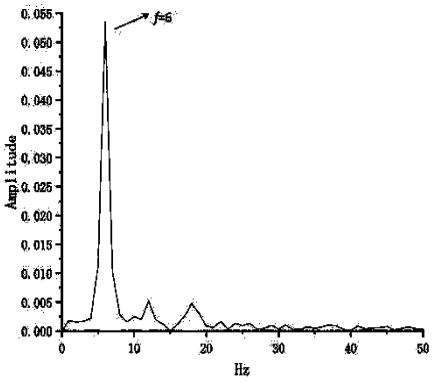

(o) Drag with α=22° and f=6.000 Hz

Fig. 14 Time domain diagram and frequency domain diagram of lift and drag coefficients of airfoil

Table 3 Excitation function of the synthetic jet at different angles of attack

Angle of attack	Expression of excitation function of synthetic jet
$\alpha = 14°$	$\left(\frac{6.5}{7.5}\right) * \sin(2\pi * 11 * t) + \left(\frac{1}{7.5}\right) * \sin(2\pi * 22 * t)$
$\alpha = 16°$	$\left(\frac{0.4}{1.2}\right) * \sin(2\pi * 0.667 * t) + \left(\frac{0.35}{1.2}\right) * \sin(2\pi * 9.607 * t) + \left(\frac{0.45}{1.2}\right) * \sin(2\pi * 10.33 * t)$
$\alpha = 19°$	$\left(\frac{12}{18.5}\right) * \sin(2\pi * 6.67 * t) + \left(\frac{4.5}{18.5}\right) * \sin(2\pi * 13 * t) + \left(\frac{2}{18.5}\right) * \sin(2\pi * 19.67 * t)$
$\alpha = 22°$	$\left(\frac{7}{25}\right) * \sin(2\pi * 3 * t) + \left(\frac{14}{25}\right) * \sin(2\pi * 6 * t) + \left(\frac{2}{25}\right) * \sin(2\pi * 11.67 * t) + \left(\frac{2}{25}\right) * \sin(2\pi * 14.67 * t)$

Table 4 Root mean square coefficients of airfoil lift and drag for a combined frequency synthetic jet exciter

Angle	Frequency	Lift (RMS)	Resistance (RMS)
14°	(6.5/7.5)*sin(2π*11*t)+(1/7.5)*sin(2π*22*t)	0.7519	0.3162
16°	(0.4/1.2)*sin(2π*0.667*t)+(0.35/1.2)*sin(2π*9.607*t)+(0.45/1.2)*sin(2π*10.33*t)	0.8264	0.3100
19°	(12/18.5)*sin(2π*6.67*t)+(4.5/18.5)*sin(2π*13*t)+(2/18.5)*sin(2π*19.67*t)	1.0614	0.4242
22°	(7/25)*sin(2π*3*t)+(14/25)*sin(2π*6*t)+(2/25)*sin(2π*11.67*t)+(2/25)*sin(2π*14.67*t)	1.0318	0.5004

According to Fig. 14 (j), the coefficient curve is aperiodic, indicating that multiple vortices are generated on the upper surface. The disturbance of the vortex near the airfoil continuously affects the trend of lift and drag. Therefore, the lift-drag ratio is not maintained at a fixed value, which means its state is in constant fluctuation. By comparing the results of Chang et al. (2022), it can be found that there is no stable lift-drag ratio in the airfoil in a chaotic state with or without the impression of a jet actuator. The attack angle of the chaotic state is increased by using a synthetic jet, but it is still possible to appear in a chaotic state under a high attack angle. Differently, it can be observed in the condition with synthetic jet exciters that the frequency of shedding vortex adjacent to the excitation frequency. This means the excitation makes the frequency of disordered shedding vortex locked around a certain value, reducing the disorder of the chaotic state.

Figure 14 (n) demonstrates that when α=22° and f=6.002 Hz, the coefficient curve varies in a sinusoidal period. After applying the jet, the structure is in 2S mode. In the spectrum diagram corresponding to the lift coefficient, the dominant frequency is 6.002 Hz, whose amplitude is close to 0.24, and the two harmonic frequencies f are 12 Hz and 18.01 Hz, respectively. The amplitudes of the two are 1/6 and 1/24.

In Fig. 14(n), at different times during the vortex-shedding cycle, although the flow field structure within the region is similar, its amplitude in the frequency domain diagram is different. In the curve graph of α=22°, it can be seen that a complete vortex shedding period has four peaks, each with different amplitudes. This means that there will be four shedding vortices with different strengths in one cycle. The different amplitudes on the coefficient curve are caused by different intensities of shedding vortices. Compared to the lift coefficient curve, the drag coefficient curve can clearly display the strength of the shedding vortex. The trough of the curve is due to the maximum capacity of the vortex at the lower edge, which is about to fall off. The curve gradually rises during the vortex shedding at the lower edge until the curve gets to the wave peak. The vortex dissipates when the curve gets to its peak. The distinct hold appearing at the wave peak is caused by vortex shedding at the upper edge. When the upper edge vortex dissipates in the filed flow, the curve begins to descend until the lower edge vortex of the next vortex falls off. The peak in the curve means that the vortex at the lower edge of the wing is shedding and dissipating, while the trough means that the vortex at the lower edge is about to fall off.

3.3 Analysis of Frequency Characteristics of Shedding Vortex under the Action of Synthetic Jet with Combined Excitation Frequency

Figure 15 (a) and (b) show that under the condition of α=14°, when synthetic jet excitation with combined frequency is adopted, the lift and drag coefficients curve still conform to sinusoidal oscillation with time. According to Fig. 15 (b), the dominant frequency is 10.5 Hz and the harmonic frequency is 20.5 Hz in the curve. The amplitude of the main frequency is about 0.195, which is four times that of the harmonic frequency. The vortex mode of the fluid field is a 2s mode.

Compared with Fig. 15 (e) of α=14°, in the case of the combined excitation frequency, the amplitude of the dominant frequency of the lift coefficient spectrum is bigger than that case of the fixed frequency. The vortex with high energy is helpful to improve the lift of the airfoil because the amplitude is proportional increase of the energy of the vortex. At this time, under the excitation of the combined frequency, the amount of harmonic frequencies in the lift coefficient spectrum is decreased from three to two. The reduction of the number of small-scale vortices indicates that the energy of the vortex is concentrated on the large-scale vortex structure. A vortex is a collection of energy, and the reduction of the small-scale vortex structure makes the fluid flowing over the wing surface provide greater lift for the wing.

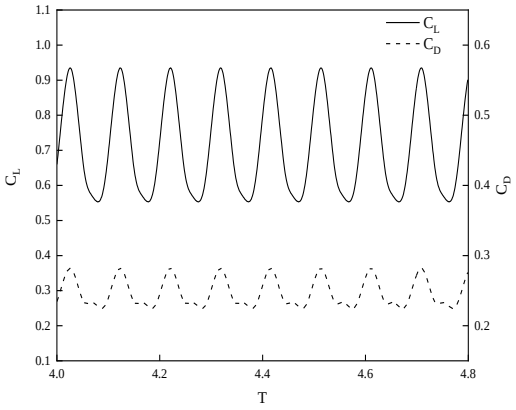

(a) α= 14°

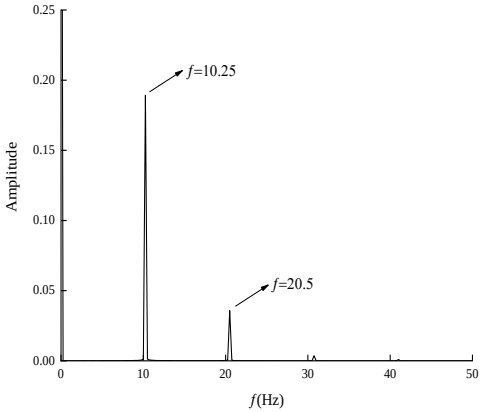

(b) Lift with α= 14°

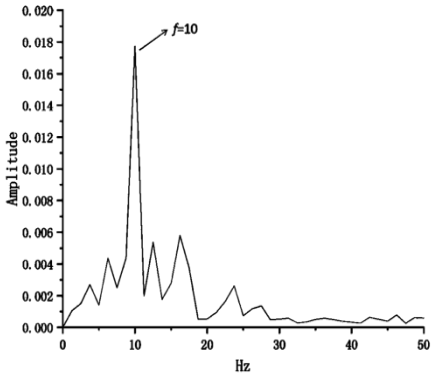

(c) Drag with α= 14°

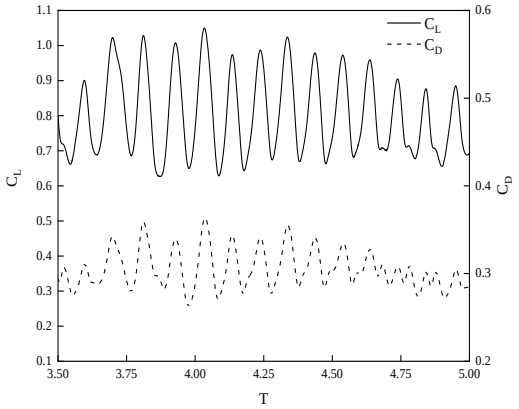

(d) α= 16°

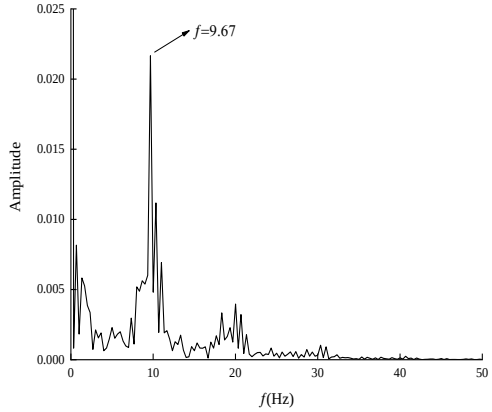

(e) Lift with α= 16°

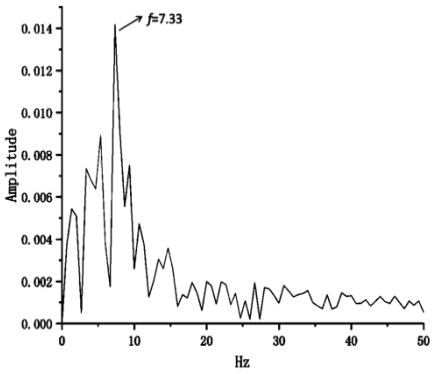

(f) Drag with α= 16°

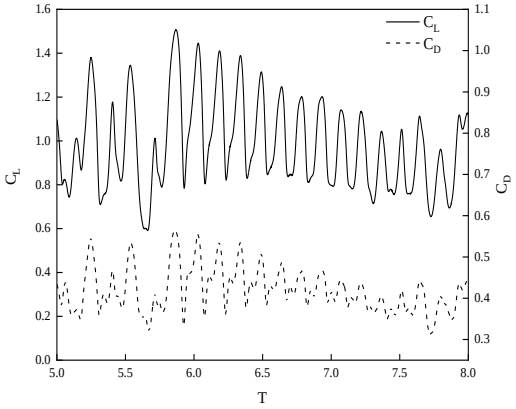

(g) α= 19°

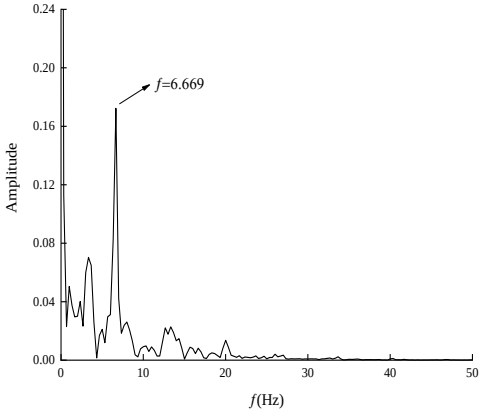

(h) Lift with α= 19°

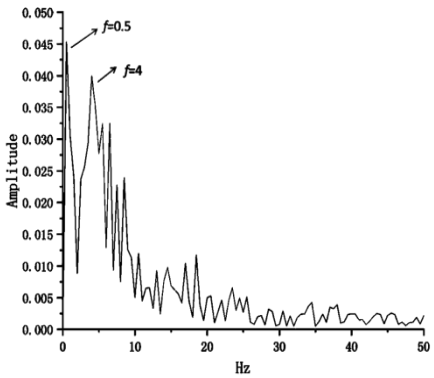

(i) Drag with α= 19°

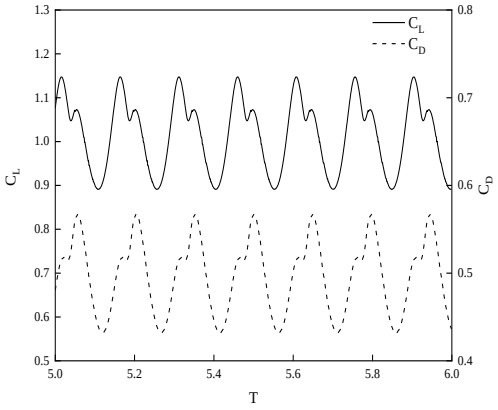

(j) α= 22 °

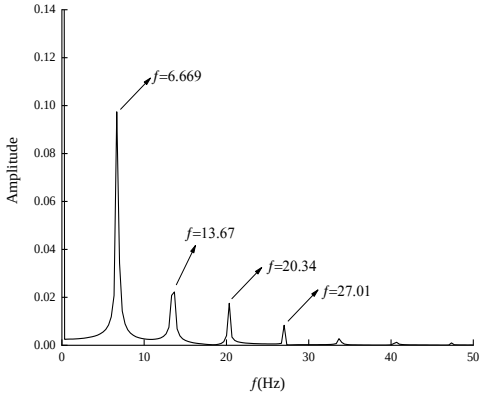

(k) Lift with α= 22 °

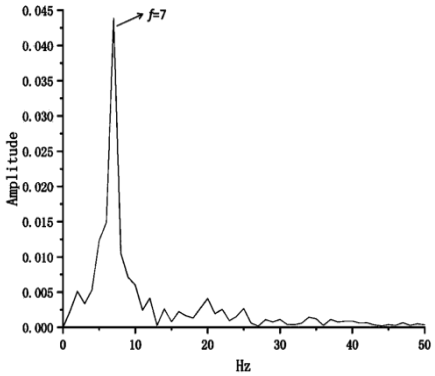

(l) Drag with α= 22 °

Fig. 15 Time domain diagram and frequency domain diagram ddr of lift and drag coefficients with multiple frequency excitation

In Fig. 15 (a), the drag coefficient is more sensitive than the lift coefficient to reflect the effect of combined frequency excitation. A small wave crest appears in the descending section of the resistance coefficient curve, which is caused by the vortex with *f*=20.5 Hz. Compared with Fig. 14 (e) of α=14°, the effect of synthetic jet with combined excitation frequency is better than fixed frequency.

According to Fig. 15 (e) of α=16°, the curves of the lift and drag coefficients of the airfoil show a quasi-sinusoidal fluctuation law, when combined frequency synthetic jet excitation is applied. Multiple frequencies with amplitudes of 0.002~0.006 appear in the lift coefficient spectrum. This shows that there are many small-scale vortex structures with similar strength but different wave frequencies near the airfoil. The main frequency corresponding to the lift coefficient is 9.670 Hz, and the amplitude is 0.022. At this time, the quasi-sinusoidal state of the lift and drag coefficient corresponds to multiple irregular frequency fluctuations of the spectrum. At α=16°, the flow state of the airfoil changes from the chaotic state without the excitation to the quasi-2S state with excitation. Compared with Fig. 14 (h), the effect of fixed dominant frequency is better than that of the combined excitation frequency.

The result of α=19° is according to Fig. 15 (g). The lift and drag coefficients still exhibit a quasi-sinusoidal wave rule. The corresponding spectrum curve is more regular than that in α=16°. The amplitude of the main frequency is about 0.17, which is lower than that of f=9.670 Hz in Fig. 15 (e) of α=16°. That is to say, at a high attack angle , the contribution of combined excitation frequency to the energy of a large-scale vortex is smaller than that of fixed frequency. As shown in Fig. 15 (h), the spectrum curve corresponding to the lift coefficient adjusts to the quasi 2S flow state law.

According to Fig. 15 (j), the curve show regular quasi-sinusoidal wave rule if α=22°. The vortex model is in a 2S (Single) state. There is one dominant frequency and three harmonic frequencies in the spectrum diagram corresponding to the lift coefficient. The values of f are 6.669 Hz, 13.67 Hz, 20.34 Hz and 27.01 Hz. The amplitude of the dominant frequency is close to 0.1, and it is lower than that at α=19°. Contrary to the effect of fixed excitation frequency, the amplitude of the corresponding dominant frequency is lower under the control of combined excitation synthetic jet when α is 16°, 19°and 22°. The contribution of a synthetic jet with fixed frequency excitation to lift is similar to that with combined frequency excitation. That is, the magnitude of the lift and drag is independent of the combination of excitation frequencies. By contrasting Fig. 14 and Fig. 15, it can be observed that for the synthetic jet with combined frequency, the lift and drag coefficient fluctuate more

regularly, and the corresponding frequency spectrum curve is also more regular.

The results show that using synthetic jets of different frequencies has a distinct impact on the frequency domain of the drag coefficient. The lift frequency domain diagrams are Fig. 14 and Fig. 15. Generally, it increases the ratio of the main frequency amplitude to all frequencies, making the fluctuation of the drag coefficient more regular. The frequency domain diagram of the resistance coefficient is shown above, and the results indicate that the use of synthetic jets with different frequencies has a distinct impact on the frequency domain of the resistance coefficient. At certain angles, the main frequency can be reduced, such as 16° and 19°. Generally, it will increase the proportion of the main frequency, making the fluctuation of the resistance coefficient more regular.

4. CONCLUSION

The paper concludes that the shedding vortex evolution law and corresponding spectral characteristics of NACA0012 airfoil are investigated at Re=10^4 and under the excitation of a jet. The impression of the jet excitation frequency on the wing vortex structure and the aerodynamic parameters of the airfoil are researched. The following research results are drawn:

(1) Under the action of a synthetic jet with a fixed frequency function, there are two modes for the unsteady state: one is a 2S state (α=10°, 14°, 16°and 22°), and the other is a chaotic state (α=19°). The angle of attack of the chaotic state changes from α=16° to α=19°, indicating that the chaotic state of the airfoil is delayed by the synthetic jet of a fixed frequency function. It is beneficial to delay the irregular vibration of airfoil triggered by flow separation at high attack angles. This improves the aerodynamic performance of airfoils at high attack angles. Jet excitation also improves the lift of airfoil significantly, especially when α=10° and α=14°.

(2) Under the action of a synthetic jet with a combined frequency function, the unsteady state is basically in 2S mode. The lift and drag oscillation law coefficients is stable when α=14°and α=22°. The lift and drag coefficients are the quasi-regular forms at α=16°and 19°. The corresponding spectrum curve is quasi 2S fluctuation law in the two cases. It shows that there are many small-scale vortex structures near the airfoil. The emergence of multiple vortex structures will weaken the energy of large-scale vortices, and the contribution of airflow to lift is reduced.

CONFLICT OF INTEREST

The authors have no conflicts to disclose.

AUTHORS CONTRIBUTION

Jiawei Wang: Visualization, Writing, Investigation, Methodology. **Xiaofeng Shi:** Project administration. **Qingui Zhang:** Investigation, Software **Jianlong. Chang:** Writing-review, Resources, Project administration, Conceptualization

REFERENCES

AlMutairi, J., ElJack, E., & AlQadi, I. (2017). Dynamics of laminar separation bubble over NACA-0012 airfoil near stall conditions. *Aerospace Science and Technology*, *68*, 193-203. https://doi.org/do10.1016/j.ast.2017.05.015

Arif, M. R., & Hasan, N. (2019a). Performance of characteristic numerical boundary conditions for mixed convective flows past a heated square cylinder using a non-Boussinesq approach. *Numerical Heat Transfer, Part A: Applications*, *76*(4), 254-280. https://doi.org/10.1080/10407782.2019.1627828

Arif, M. R., & Hasan, N. (2019b). Vortex shedding suppression in mixed convective flow past a square cylinder subjected to large-scale heating using a non-Boussinesq model. *Physics of Fluids*, *31*(2), https://doi.org/10.1063/1.5079516

Arif, M. R., & Hasan, N. (2020). Large-scale heating effects on global parameters for flow past a square cylinder at different cylinder inclinations. *International Journal of Heat and Mass Transfer*, *161*, 120237. https://doi.org/10.1016/j.ijheatmasstransfer.2020.120237.

Arif, M. R., & Hasan, N. (2021). Effect of free-stream inclination and buoyancy on flow past a square cylinder in large-scale heating regimes. *Physics of Fluids*, *33*(7). https://doi.org/10.1063/5.0054766

Cao, S., Dang, N., Ren, Z., Zhang, J., & Deguchi, Y. (2020). Lagrangian analysis on routes to lift enhancement of airfoil by synthetic jet and their relationships with jet parameters. *Aerospace Science and Technology*, *104*, 105947. https://doi.org/10.1016/j.ast.2020.105947.

Chang, J., Zhang, Q., He, L., & Zhou, Y. (2022). Shedding vortex characteristics analysis of NACA 0012 airfoil at low Reynolds numbers. *Energy Reports*, *8*, 156-174. https://doi.org/10.1016/j.egyr.2022.01.149

Couto, N., & Bergada, J. M. (2022). Aerodynamic efficiency improvement on a NACA-8412 airfoil via active flow control implementation. *Applied Sciences*, *12*(9), 4269. https://doi.org/10.3390/app12094269

Di Ilio, G., Chiappini, D., Ubertini, S., Bella, G., & Succi, S. (2018). Fluid flow around NACA 0012 airfoil at low-Reynolds numbers with hybrid lattice Boltzmann method. *Computers & Fluids*, *166*, 200-208. https://doi.org/10.1016/j.compfluid.2018.02.014

Di, G., Wu, Z., & Huang, D. (2017). The research on active flow control method with vibration diaphragm on a NACA0012 airfoil at different stalled angles of attack. *Aerospace Science and Technology*, *69*, 76-86. https://doi.org/10.1016/j.ast.2017.06.020

Fala, N. (2022). An analysis of fixed-wing stall-type

accidents in the United States. *Aerospace*, *9*(4), 178. https://doi.org/10.3390/aerospace9040178

Feero, M. A., Goodfellow, S. D., Lavoie, P., & Sullivan, P. E. (2015). Flow reattachment using synthetic jet actuation on a low-Reynolds-number airfoil. *AIAA Journal*, *53*(7), 2005-2014. https://doi.org/10.2514/1.J053605

Feero, M. A., Lavoie, P., & Sullivan, P. E. (2017). Influence of synthetic jet location on active control of an airfoil at low Reynolds number. *Experiments in Fluids*, *58*, 1-12. https://doi.org/10.1007/s00348-017-2387-x

Goodarzi, M., Rahimi, M., & Fereidouni, R. (2012). Investigation of active flow control over NACA0015 airfoil via blowing. *International Journal of Aerospace Sciences*, *1*(4), 57-63 https://doi.org/10.5923/j.aerospace.20120104.01

Goodfellow, S. D., Yarusevych, S., & Sullivan, P. (2010, January). *Low Reynolds number flow control over an airfoil using synthetic jet actuators*. ASME International Mechanical Engineering Congress and Exposition (Vol. 44441, pp. 909-915). https://doi.org/10.1115/IMECE2010-39728

Gupta, S., Zhao, J., Sharma, A., Agrawal, A., Hourigan, K., & Thompson, M. C. (2023). Two-and three-dimensional wake transitions of a NACA0012 airfoil. *Journal of Fluid Mechanics*, *954*, A26. https://doi.org/10.1017/jfm.2022.958

Han, L., Wei, D., Wang, Y., & Zhang, X. (2021). Vortex-induced vibration mechanism of the NACA 0012 airfoil based on a method of separating disturbances. *Journal of Sound and Vibration*, *501*, 116044. https://doi.org/10.1016/j.jsv.2021.116044

Itsariyapinyo, P., & Sharma, R. (2016). *NACA0015 circulation control airfoil using synthetic jets at low angles of attack and low reynolds number*. 8th AIAA Flow Control Conference. https://doi.org/10.2514/6.2016-3772

Khan, M. A., Masood, S., Anwer, S. F., Khan, S. A., & Arif, M. R. (2023). Vortex induced vibration for mixed convective flow past a square cylinder. *International Journal of Heat and Mass Transfer*, *202*, 123722. https://doi.org/10.1016/j.ijheatmasstransfer.2022.123722

Kim, D. H., & Chang, J. W. (2014). Low-Reynolds-number effect on the aerodynamic characteristics of a pitching NACA0012 airfoil. *Aerospace Science and Technology*, *32*(1), 162-168. https://doi.org/10.1016/j.ast.2013.08.018

Kim, D. H., Yang, J. H., Chang, J. W., & Chung, J. (2009, January). *Boundary layer and near-wake measurements of NACA 0012 airfoil at low Reynolds numbers.* 47th AIAA Aerospace Sciences Meeting Including the New Horizons Forum and Aerospace Exposition. https://doi.org/10.2514/6.200

Kim, M., Essel, E. E., & Sullivan, P. E. (2022). Effect of varying frequency of a synthetic jet on flow separation over an airfoil. *Physics of Fluids*, *34*(1). pp. https://doi.org/10.1063/5.0077334

Klochkov, V. V., & Kritskaya, S. S. (2017). Forecasting the impact of economic sanctions on the development of the Russian aircraft industry. *Studies on Russian Economic Development*, *28*, 616-623. https://doi.org/10.1134/S107570071706003X

Kurtulus, D. F. (2015). On the unsteady behavior of the flow around NACA 0012 airfoil with steady external conditions at Re= 1000. *International journal of micro air vehicles*, *7*(3), 301-326. https://doi.org/10.1260/1756-8293.7.3.301

Kurtulus, D. F. (2019). Unsteady aerodynamics of a pitching NACA 0012 airfoil at low Reynolds numbers. *International Journal of Micro Air Vehicles*, *11*, 1756829319890609. https://doi.org/10.1177/1756829319890609

Lei, J., Zhang, J., & Niu, J. (2020). Effect of active oscillation of local surface on the performance of low Reynolds number airfoil. *Aerospace Science and Technology*, *99*, 105774. https://doi.org/10.1016/j.ast.2020.105774

Lindstrom, A., Monastero, M., & Amitay, M. (2018). *The flow physics of synthetic jets interaction with flow over a flapped airfoil*. 2018 Flow Control Conference. https://doi.org/10.2514/6.2018-4019

Lou, B., Ye, S., Wang, G., & Huang, Z. (2019). Numerical and experimental research of flow control on an NACA 0012 airfoil by local vibration. *Applied Mathematics and Mechanics*, *40*(1), 1-12. https://doi.org/10.1007/s10483-019-2404-8

Monastero, M. C., & Amitay, M. (2016). *Performance enhancement of an airfoil model with a control surface using synthetic jets*. 8th AIAA Flow Control Conference. https://doi.org/10.2514/6.2016-3305

Monastero, M. C., Lindstrom, A. M., & Amitay, M. (2019). Effect of synthetic jet spacing on flow separation over swept, flapped airfoils. *AIAA Journal*, *57*(11), 4670-4683. https://doi.org/10.2514/1.J058304

Moshfeghi, M., & Hur, N. (2017). Numerical study on the effects of a synthetic jet actuator on S809 airfoil aerodynamics at different flow regimes and jet flow angles. *Journal of Mechanical Science and Technology*, *31*, 1233-1240. https://doi.org/10.1007/s12206-017-0222-1

Nedić, J., & Vassilicos, J. C. (2015). Vortex shedding and aerodynamic performance of airfoil with multiscale trailing-edge modifications *AIAA Journal*, *53*(11), 3240-3250. https://doi.org/10.2514/1.J053834

Neve, M., Kalamkar, V. R., & Wagh, A. (2017, December). *Numerical analysis of NACA aerofoil using synthetic jet*. In Gas Turbine India Conference (Vol. 58509, p. V001T01A006). American Society of Mechanical Engineers. https://doi.org/10.1115/GTINDIA2017-4587

Nguyen, D. H., Lowenberg, M. H., & Neild, S. A. (2022). A Frequency-Domain Approach to Analysing Dynamic Deep Stall Recovery. In *AIAA SCITECH 2022 Forum* (p. 1935). https://doi.org/10.2514/6.2022-1935.

Pradhan, A., Arif, M. R., Afzal, M. S., & Gazi, A. H. (2022). On the origin of forces in the wake of an elliptical cylinder at low Reynolds number. *Environmental Fluid Mechanics*, *22*(6), 1307-1331. https://doi.org/10.1007/s10652-022-09892-z

Rodríguez, I., Lehmkuhl, O., Borrell, R., & Oliva, A. (2013). Direct numerical simulation of a NACA0012 in full stall. *International Journal of Heat and Fluid Flow*, *43*, 194-203. https://doi.org/10.1016/J.IJHEATFLUIDFLOW.2013.05.002

Saadi, M. C., & Bahi, L. (2018). Effect of jet width and momentum coefficient of active control over NACA0012 airfoil using synthetic jet. *Journal Homepage*, *36*(4), 1443-1449. https://doi.org/10.18280/ijht.360437

Shan, H., Jiang, L., Liu, C., Love, M., & Maines, B. (2008). Numerical study of passive and active flow separation control over a NACA0012 airfoil. *Computers & fluids*, *37*(8), 975-992. https://doi.org/10.1016/j.compfluid.2007.10.010

Shen, X., Avital, E., Rezaienia, M. A., Paul, G., & Korakianitis, T. (2017). Computational methods for investigation of surface curvature effects on airfoil boundary layer behavior. *Journal of Algorithms & Computational Technology*, *11*(1), 68-82. https://doi.org/10.1177/1748301816665527

Singh, D. K., Jain, A., & Paul, A. R. (2021). Active flow control over a NACA23012 airfoil using hybrid jets. *Defence Science Journal*, *71*(6), 721-729. https://doi.org/10.14429/DSJ.71.16468

Tadjfar, M., & Kamari, D. (2020). Optimization of flow control parameters over SD7003 airfoil with synthetic jet actuator. *Journal of Fluids Engineering*, *142*(2), 021206. https://doi.org/10.1115/1.4044985

Tang, Z. L., Sheng, J. D., Zhang, G. D., & Periaux, J. (2018). Large-scale separation flow control on airfoils with synthetic jet. *International Journal of Computational Fluid Dynamics*, *32*(2-3), 104-120. https://doi.org/10.1080/10618562.2018.1508656

Wang, C., & Tang, H. (2018). Enhancement of aerodynamic performance of a heaving airfoil using synthetic-jet based active flow control. *Bioinspiration & Biomimetics*, *13*(4), 046005. https://doi.org/10.1088/1748-3190/aabdb9

Wang, J., & Wu, J. (2020). Aerodynamic performance improvement of a pitching airfoil via a synthetic jet. *European Journal of Mechanics-B/Fluids*, *83*, 73-85. https://doi.org/10.1016/j.euromechflu.2020.04.009

Wu, J. Z., Lu, X. Y., Denny, A. G., Fan, M., & Wu, J. M. (1998). Post-stall flow control on an airfoil by local unsteady forcing. *Journal of Fluid Mechanics*, *371*, 21-58. https://doi.org/10.1017/S0022112098002055

Yang, E., Ekmekci, A., & Sullivan, P. E. (2022). Phase evolution of flow controlled by synthetic jets over NACA 0025 airfoil. *Journal of Visualization*, *25*(4), 751-765. https://doi.org/10.1007/s12650-021-00824-5

Yarusevych, S., Sullivan, P. E., & Kawall, J. G. (2009). On vortex shedding from an airfoil in low-Reynolds-number flows. *Journal of Fluid Mechanics*, *632*, 245-271. https://doi.org/10.1017/S0022112009007058

Yen, S. C., & Hsu, C. M. (2007). Investigation on vortex shedding of a swept-back wing. *Experimental Thermal and Fluid Science*, *31*(8), 849-855. https://doi.org/10.1016/j.expthermflusci.2006.09.001

You, D., & Moin, P. (2008). Active control of flow separation over an airfoil using synthetic jets. *Journal of Fluids and Structures*, *24*(8), 1349-1357. https://doi.org/10.1016/j.jfluidstructs.2008.06.017

Zhang, W., & Samtaney, R. (2015). A direct numerical simulation investigation of the synthetic jet frequency effects on separation control of low-Re flow past an airfoil. *Physics of Fluids*, *27*(5), https://doi.org/10.1063/1.4919599

Zhang, Z., Wang, T., Wang, Y., & Guo, H. (2020, July). *Effect of suction and blowing control on NACA 0012 airfoil at low Reynolds number*. Journal of Physics: Conference Series (Vol. 1600, No. 1, p. 012040). IOP Publishing. https://doi.org/10.1088/1742-6596/1600/1/012040